Optical Materials 34 (2012) 536–554

Contents lists available at ScienceDirect

Optical Materials

journal homepage: www.elsevier.com/locate/optmat

Parametric down-conversion devices: The coverage of the mid-infrared spectral range by solid-state laser sources

Valentin Petrov

Max-Born-Institute for Nonlinear Optics and Ultrafast Spectroscopy, 2A Max-Born-Str., D-12489 Berlin, Germany

ARTICLE INFO

Article history:
Received 11 November 2010
Accepted 21 March 2011
Available online 30 April 2011

Keywords:
Parametric down-conversion
Mid-infrared
Nonlinear crystals
Difference-frequency generation
Optical parametric oscillators
Optical parametric generators and amplifiers

ABSTRACT

The development of parametric down-conversion devices operating in the mid-infrared, from 3 μm to about 20 μm, based on non-oxide nonlinear optical crystals is reviewed. Such devices, pumped by solid-state laser systems operating in the near-infrared, fill in this spectral gap where no solid-state laser technology exists, on practically all time scales, from continuous-wave to femtosecond regime. The vital element in any frequency-conversion process is the nonlinear optical crystal and this represents one of the major limitations with respect to achieving high energies and average powers in the mid-infrared although the broad spectral tunability seems not to be a problem. Hence, an overview of the available mid-infrared nonlinear optical materials, emphasizing new developments like wide band-gap, engineered (mixed), and quasi-phase-matched crystals, is also included.

1. Introduction: up- and down-conversion of the laser frequency by second-order nonlinear processes in noncentrosymmetric crystals

The discovery and development of nonlinear optical phenomena were only possible after the invention of the laser. At the relatively low light intensities that normally occur in nature, the optical properties of materials are quite independent of the light intensity and there is no interaction between the waves. However, if the light intensity is sufficiently high, the optical properties begin to depend on it and other light characteristics. Thus, the light waves may interact with a transparent dielectric medium and with each other. Such effects are utilized in nonlinear-optical devices and techniques to convert the wavelength of existing lasers.

In the absence of dispersion, linear optical phenomena are described by the simple relation

$$\vec{P} = \varepsilon_0 \chi^{(1)} \vec{E} \tag{1}$$

between the polarization and the electric field, where ε_0 is the dielectric constant and $\chi^{(1)}$ denotes the linear susceptibility. The most general relation in the case of nonlinear optics (spatial dispersion neglected) reads:

$$\begin{aligned}\vec{P}(t) &= \vec{P}_L(t) + \vec{P}_{NL}(t) \\ &= \varepsilon_0 \int_{-\infty}^{t} \chi^{(1)}(t;t_1)\vec{E}(t_1)dt_1 + \varepsilon_0 \\ &\times \int\int_{-\infty}^{t} \chi^{(2)}(t;t_1,t_2)\vec{E}(t_1)\vec{E}(t_2)dt_1dt_2 + \varepsilon_0 \\ &\times \int\int\int_{-\infty}^{t} \chi^{(3)}(t;t_1,t_2,t_3)\vec{E}(t_1)\vec{E}(t_2)\vec{E}(t_3)dt_1dt_2dt_3 \cdots\end{aligned} \tag{2}$$

and includes the nonlinear susceptibilities of 2nd, 3rd and higher orders. Assuming interaction far from resonances, no losses and no dispersion (instantaneous medium response), the above relation is simplified and the susceptibilities become constants:

$$\vec{P} = \vec{P}_L + \vec{P}_{NL} = \varepsilon_0\left(\chi^{(1)}\vec{E} + \chi^{(2)}\vec{E}\vec{E} + \chi^{(3)}\vec{E}\vec{E}\vec{E} + \cdots\right) \tag{3}$$

Here, only three-photon nonlinear processes will be considered, the lowest order second-order nonlinear processes, which are described by the second term in the above equation. It is obvious that in the presence of two waves with different carrier frequencies this term will cause the polarization to have terms oscillating at the sum- and difference-frequencies. It can be shown that the second-order susceptibility tensor $\chi^{(2)}$ is non-zero only in media without an inversion center (acentric or noncentrosymmetric materials). Second-harmonic generation (SHG), also called frequency doubling, is the simplest such nonlinear optical process, in which photons interacting with a nonlinear material (noncen-

E-mail address: petrov@mbi-berlin.de

0925-3467/$ - see front matter © 2011 Elsevier B.V. All rights reserved.
doi:10.1016/j.optmat.2011.03.042

trosymmetric crystal) are effectively "combined" to form new photons with twice the energy, and therefore twice the frequency and half the wavelength of the initial photons. SHG was also the first nonlinear optical process demonstrated in 1961 by Franken et al. at the University of Michigan [1], just 1 year after the discovery of the ruby laser by Maiman at Hughes Research Laboratories. It was this solid-state laser that was used in the first SHG experiment with quartz as the nonlinear optical crystal. While 10^{-8} photon conversion efficiency was achieved in this first SHG experiment, which corresponds to 3×10^{-10}%/W, at present the improvement using engineered nonlinear devices is by more than 12 orders of magnitude.

Soon afterwards the theory of the more general optical parametric three-wave interactions was developed. The generation of a photon at frequency ω_1 when photons at frequencies ω_3 and ω_2 are incident on a crystal with non-zero second-order susceptibility $\chi^{(2)}$, such that $\omega_1 = \omega_3 - \omega_2$ (assuming $\omega_3 > \omega_2$), is called Difference-Frequency Generation (DFG). In order for energy conservation to hold, this additionally implies that, for every photon generated at the difference frequency ω_1, a photon at ω_2 must also be created, while a photon at the higher frequency ω_3 must be annihilated. In addition, for the process to take place with an appreciable efficiency of frequency conversion, phase-matching must occur, so that $\vec{k}_1 = \vec{k}_3 - \vec{k}_2$. For collinear interaction, this equation is equivalent to $n_1\omega_1 = n_3\omega_3 - n_2\omega_2$, where n_i are the corresponding refractive indices. This condition is impossible to satisfy in isotropic (cubic) materials but the dispersion can be balanced by birefringence in anisotropic materials and this is the so-called angle phase-matching, the most common method to satisfy the above relation by using waves of different polarization. In this case the equations for the three waves are coupled and the conversion efficiency is determined by the so called effective nonlinearity d_{eff} which is some linear combination of components of the nonlinearity tensor $d_{il} = \chi^{(2)}_{il}/2$ depending on the propagation direction (polar angle θ and azimuthal angle φ), which is derived from the phase-matching condition, and the corresponding polarizations. For propagation along (in biaxial crystals) or perpendicular (in uniaxial crystals) to a crystal optical axis, there is no spatial walk-off of the interacting waves and tight focusing can be used with long crystal samples, essential for low power, e.g. continuous-wave (cw) operation. This is the so-called noncritical phase-matching (NCPM) which is often compatible also with maximum d_{eff}. In the absence of phase-matching the energy flows back and forth, and not in the desired direction from the pump wave to the other waves, with a period of $2L_c$ where the coherence length L_c is given by $\pi/|\Delta k|$ and $|\Delta k| = |k_3 - k_2 - k_1|$ is the phase-mismatch in the case of collinear propagation. However, there is a possibility to keep the energy flow "almost" in the same direction by the so-called quasi-phase-matching (QPM) if the nonlinear crystal (NLC) is divided into segments each a coherence length long and then rotated relative to its neighbors by 180° about the axis of propagation which, because of the lack of inversion symmetry, has the effect of changing the sign of all components d_{il} and hence of d_{eff}. Bonding of such plates into a stack is obviously one possible realization of QPM but a more elegant way in the case of ferroelectric materials is electric field poling. QPM not only enables the use of highly nonlinear isotropic (or also low birefringent) semiconductors, it is in principle NCPM and in addition utilizes diagonal elements of d_{il} which are in general larger. For short wavelengths, L_c could be very short and one can use odd multiple of L_c for each slab. However, in the mid-infrared (mid-IR) this is not necessary and the nonlinearity of the process for the lowest (first) order grating is given simply by $(2/\pi)d_{\text{eff}}$.

DFG is the basic nonlinear process for down-conversion, i.e. to transfer the power (energy) from a strong laser field at ω_3 to lower frequencies (longer wavelengths). The opposite process, Sum-Frequency Generation (SFG), see Table 1, is used for up-conversion and SHG is a particular case of SFG. Since the mid-IR spectral range can be approached with solid-state-laser (SSL) technology only starting from shorter wavelengths, this is achieved basically by down-conversion. Note that down-conversion devices (see Table 1) are in general more difficult to realize because there is a certain threshold for the field at ω_3 which is not the case for SFG, however, DFG offers in general also wider wavelength tunability of the resulting lower-frequency fields.

In many situations of DFG, the field at ω_3 is an intense pump field, while the field at ω_2 is a weak signal field. DFG yields amplification of the ω_2 field (along with generation of another field at ω_1, commonly called the idler field). Thus, this process is termed parametric amplification. The parametric gain depends on the NLC length, pump intensity and d_{eff}. Another essential characteristic is the parametric gain bandwidth which gives the range of signal wavelengths that experience amplification.

Table 1
Systematics of $\chi^{(2)}$- or three-photon-processes: lowest order nonlinear effects in noncentrosymmetric media. The convention $\omega_1 \leqslant \omega_2 < \omega_3$ ($\lambda_1 \geqslant \lambda_2 > \lambda_3$) is used. The third column summarizes the characteristics of up- and down-conversion parametric devices.

SFG (Sum-Frequency Generation)	$\omega_3 = \omega_2 + \omega_1$ (energy conservation) $\hbar\omega_1$, $\hbar\omega_2$ annihilated, $\hbar\omega_3$ created	SFG (Mixing): feasible on all time scales (from cw to fs); requires two laser sources, synchronization, but no threshold; the conversion efficiency can be very high
SHG (second harmonic generation):	$\omega_3 = 2\omega_1 \equiv$ SFG ($\omega_1 = \omega_2$)	Particular case of SFG
DFG (Difference-Frequency Generation)	$\omega_1 = \omega_3 - \omega_2$ (or $\omega_2 = \omega_3 - \omega_1$) $\hbar\omega_3$ annihilated, $\hbar\omega_2$, $\hbar\omega_1$ created input ω_2, wave is amplified (parametric amplification)	DFG (Mixing): feasible on all time scales (from cw to fs); requires two laser sources, synchronization; the conversion efficiency is relatively low
OPG (optical parametric generation)	Only pump wave at ω_3 present and two new waves at ω_1 and ω_2 (idler and signal) generated from parametric noise	OPG (Generator): no input signal, output from amplification of parametric noise; requires high intensity (ps or fs pulses) but has high gain and can tolerate certain losses (e.g. residual absorption, Fresnel reflections)
OPA (optical parametric amplification) DFG ≡ OPA (???)	≡ OPG + (weak) seed wave @ ω_2 or ω_1. Gain (DFG) ≈ 1 e.g. @ ω_2 Gain (OPA) ≫ 1 e.g. @ ω_2	OPA (Amplifier): input signal provided which reduces the threshold and improves the spectral, temporal and spatial properties; otherwise as OPG
OPO (optical parametric oscillation)	≡ (OPG or OPA) + resonator	OPO (Oscillator): SRO or DRO; pump: single-pass, double-pass, resonated, or intracavity pumped; long pulse or cw (many round trips): from ns to cw, can be seeded to reduce threshold or improve spectral properties
SPOPO (synchronously pumped OPO)	Requires cw or long (typically μs) train of ultrashort (ps or fs) pulses from a mode-locked laser oscillator operating in the steady-state or burst mode	SPOPO: low threshold average power, synchronized outputs at two wavelengths, very high gain possible, can oscillate even with very high idler loss, very high efficiency, e.g. cascaded SPOPOs are practical

If this process occurs within an optical cavity with resonance frequency ω_2, the device is called an Optical Parametric Oscillator, or OPO. If the cavity has modes at both ω_2 and ω_1, the device is a Doubly-Resonant OPO, Fig. 1b. DFG can also occur in the absence of an applied signal field; under these circumstances, it is called Spontaneous Parametric Fluorescence. In this case, the frequencies of the generated photons are determined by the phase-matching condition for the particular crystal orientation used.

The first OPO, based on $LiNbO_3$, was demonstrated in 1965 by Giordmaine et al. at Bell Telephone Laboratories [2]. It utilized the high power of a short pulse (nanosecond) Nd:$CaWO_4$ laser operating in the Q-switched (giant-pulse) regime. Continuous-wave OPOs were realized in the following years: at first doubly resonant to reduce the pump threshold and later singly resonant – to avoid the instabilities and complex tuning. Another option to reduce the threshold in OPOs is intracavity pumping. While OPO is a feasible concept from nanosecond time scale to cw operation, the parametric down-conversion of ultrashort (picosecond and femtosecond) laser pulses can be realized in "single-pass" traveling-wave schemes, called Optical Parametric Generator (OPG) when the process is initiated by the Spontaneous Parametric Fluorescence and Optical Parametric Amplifier (OPA) when a weak signal wave is amplified, Fig. 1a. OPG presents the simplest set-up but offers less control on the output properties and requires high pump intensities which are often close to the NLC damage threshold. OPA is really not different from DFG except that one has in mind that the input wave at ω_2 is weak and is to be strongly amplified.

DFG is applicable on any time scale (from femtosecond to cw) but requires two wavelengths and the conversion efficiency to the idler wave is rather low. OPO, OPA and OPG can produce high conversion efficiencies leading to depletion of the pump power. In these devices, Q-switched nanosecond lasers or ultrafast amplifiers are normally used for high-energy parametric down-conversion of nanosecond, picosecond and femtosecond pulses while the repetition rate varies from a few Hz up to about 1 MHz. Low energy picosecond and femtosecond pulses from mode-locked laser oscillators

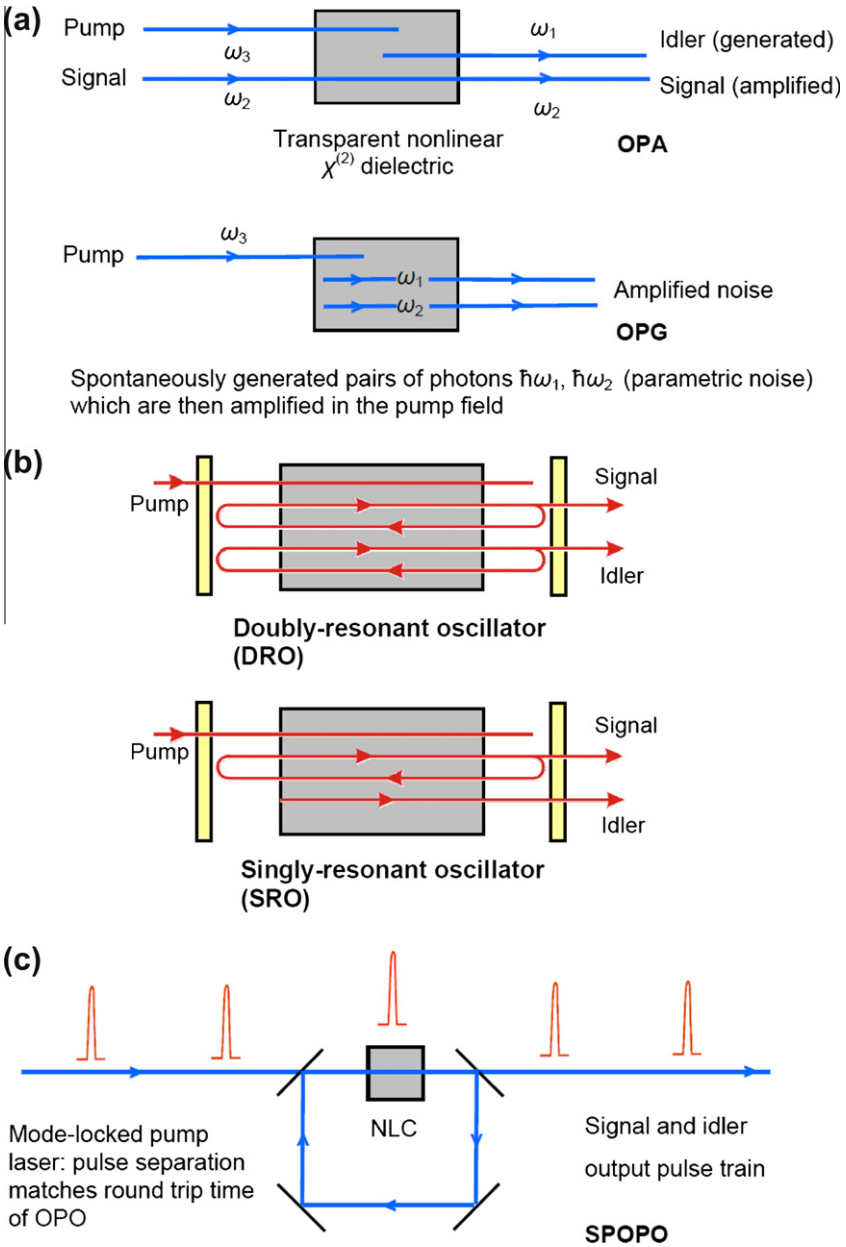

Fig. 1. Down-conversion devices: (a) OPA and OPG, (b) OPO, and (c) SPOPO.

can be down-converted employing an OPO cavity with a length matched to the repetition rate of the pump source (from ~50 MHz to ~1 GHz). These devices are called Synchronously Pumped OPO (SPOPO), Fig. 1c. It should be emphasized that in all down-conversion devices operating with ultrashort (i.e. picosecond or femtosecond) pulses, the NLC length must be short enough so that group velocity mismatch (GVM) does not separate pump, signal and idler pulses in the crystal.

All the above parametric down-conversion processes and devices have their laser analogs and there are many similarities with the operation of a laser. However, there are also essential differences: (i) parametric devices require coherent pump sources, i.e. lasers, and parametric fluorescence and gain occur in the direction of the pump beam (no analog of side-pumped lasers), there is a finite range of pump wave directions at which the signal wave is amplified and multimode pump sources can be used (brightness enhancement), (ii) their wavelength is determined and tuning is realized by changing the phase-matching conditions (change of crystal tilt or temperature or grating period in the case of QPM), the signal-idler tuning is very broad with possibility to access wavelengths where no lasers exist such as mid-IR, far-IR or THz, and the spectral gain-bandwidth is defined by the dispersive properties of the NLC and its length, (iii) no heat is deposited in a NLC unless there is some residual absorption at some of the three wavelengths involved, there is no energy exchange with the nonlinear medium – only exchange between the interacting waves, (iv) there is no gain/energy storage in the NLC because no levels are occupied and the dynamics is completely different due to the instantaneous nature of the nonlinear process: gain is only present while pump is present and as a consequence the temporal profile of the output is determined to a great extent by the temporal profile of the pump and seed (signal) radiation as well as by the dispersive properties of the NLC, (v) gain is produces at two-wavelengths – two outputs, (vi) gain is determined by peak pump intensity and very high gain is possible with ultrashort pump pulses.

The tuning capability of parametric down-conversion devices is a major advantage because it can be not only much broader than any tunable laser but can cover wavelength ranges inaccessible to (solid-state) lasers.

Since the pioneering work of Franken et al. on SHG, parametric down-conversion and up-conversion processes in NLCs as well as combinations of them have been widely used to fill in gaps in the optical spectrum where lasers do not exist or certain operational regimes are impossible: from the vacuum ultraviolet (~150 nm) to the deep mid-IR. The main progress took place in the last two decades following the advancement in near-infrared SSL technology and nonlinear optical crystals.

2. The mid-infrared spectral range: non-oxide nonlinear materials

There is no unique definition of the mid-IR spectral range but one can adopt it consists of the mid-wavelength IR (MWIR) range extending from 3 to 8 μm and the long-wavelength IR (LWIR) extending from 8 to 15 μm while the far-IR begins from 15 μm. The applications of coherent mid-IR sources include (i) Detection and quantification of molecular trace gases: the spectral region of fundamental vibrational molecular absorption bands from 3 to 20 μm is the most suitable for high sensitivity trace gas detection (DFG, OPO); (ii) Military applications: directed infrared countermeasures (DIRCM) in the 4–5 μm spectral range, jamming heat-seeking MANPADS (high power OPO); (iii) Medical applications: e.g. minimally invasive neurosurgery (tissue ablation) in the 6.1–6.45 μm range requiring high single pulse energy OPOs at <1 kHz repetition rate; (iv) Evaporation and thin-film deposition of polymers: resonant infrared (RIR) pulsed laser deposition (PLD) preserving the structure of the target material (OPOs and SPOPOs); (v) Spectroscopy and other scientific applications: Both high-resolution and time resolved, e.g. excite and probe vibrational transitions in molecules or intersubband transitions in semiconductor structures (OPG, OPA, DFG, SPOPO).

The entire mid-IR spectral range is a very wide "gap" where only few gas but no SSLs exist. Indeed, the upper limit of practical SSLs, such as Er^{3+} or Cr^{2+}, extends to about 3 μm. Other transitions at longer wavelengths exist but temperature quenching of the mid-IR fluorescence (Fe^{2+}) or the lack of suitable pump sources represent basic limitations. In most cases operation at low temperature and/or using pulsed pumping (e.g. for Dy^{3+}) is required. A recent review on the development of transition-metal mid-IR lasers reports impressive progress [3], nevertheless, it is hard to imagine that all temporal regimes (from cw down to femtosecond) will be ever realized with mid-IR SSLs which often exhibit only narrow band emission (e.g. Nd^{3+} or Pr^{3+}).

Thus, at present the main approach to cover the mid-IR spectral range on the basis of all-SSL technology is down-conversion employing NLCs. There are oxide crystals that are partially transparent in the mid-IR but not more than 4–5 μm. Indeed, the performance of oxide based crystals is affected by multiphonon absorption starting in the best case from about 4 μm and thus non-oxide materials have to used, such as unary, binary, ternary and quaternary arsenides, phosphides, sulfides, selenides or tellurides. Some of these inorganic crystals transmit up to 20–30 μm before multiphonon absorption occurs as an intrinsic limit. In contrast with the oxides, which can be grown by well mastered and harmless hydrothermal, flux or Czochralski methods, the more complex Bridgman–Stockbarger growth technique in sealed (high atmosphere) ampoules, with volatile and chemically reactive starting components, is the only method used to produce large size single domain non-oxide crystals, and this certainly hampered their development all the more that special post-growth treatments are needed to restore stoichiometry and improve their optical quality. As a matter of fact such materials exhibit more defects and the residual losses (absorption and scatter) are more than one order of magnitude larger than in the best oxide crystals.

Note that the longer the long-wave transmission limit the smaller the band-gap of such non-oxide materials which means that down-conversion will require laser pump sources operating at longer wavelengths, or if such do not exist, cascaded schemes based on oxides in the first stage. This restriction is even more pronounced when using short (nanosecond) and ultrashort (picosecond or femtosecond) pulses for pumping non-oxide materials because of the detrimental role of two-photon absorption (TPA), a higher order nonlinear effect, which sets the limit for the pump wavelength to half the band-gap value $\sim E_g/2$. Thus, e.g. only very few materials can be used for direct conversion of femtosecond pulses from Ti:sapphire laser systems operating near 800 nm and cascaded parametric down-conversion schemes are required. Even for wavelengths in the 1-μm spectral range, where powerful Nd^{3+} or Yb^{3+} nanosecond and picosecond laser systems exist, limitations related to the residual loss, nonlinearity, phase-matching, thermo-mechanical properties, or simply growth and availability, do not allow one to generate high single pulse energies and/or average powers in the mid-IR. In such cases pumping at longer wavelengths (e.g. by Er^{3+} lasers near 1.5 μm, Tm^{3+} and Ho^{3+} lasers near 2 μm, Er^{3+} lasers near 2.9 μm or cascaded schemes) has to be used.

There are exceptions of widely transmitting mid-IR NLCs such as the ternary halides whose short-wave limit extends down to the ultraviolet (UV) [4] but estimations of the nonlinear coefficients d_{il} of these materials (until now only by the powder SHG method) show that the values do not exceed 1 pm/V. On the

contrary, typical mid-IR NLCs exhibit nonlinear coefficients on the order of 10 pm/V or above, in the best cases few tens of pm/V, with the record value of ~600 pm/V for Te. There are fundamental relations between the nonlinearity and the index of refraction and although d_{il} may vary a lot, the quantity $\delta = d_{il}/(n^2-1)^3 = d_{il}/(\chi^{(1)}-1)^3$ (Miller's delta) remains almost constant (e.g. within one order of magnitude, Miller's empirical rule) [5]. Mid-IR NLCs have $n > 2$ and empirical formulae indicate that the index of refraction depends on the material bandgap as $\sim E_g^{-1/4}$ [5], hence, at $n \gg 1$, $d \sim E_g^{-3/2}$ (here d is some average nonlinearity). The index of refraction also enters the expression for the coupling constant in three-photon interaction equations and it is not the d-tensor that should be compared for different materials but rather some figure of merit, such as FM $\sim d^2/n^3$, which determines the conversion efficiency. Thus, at $n \gg 1$, FM $\sim n^9 \sim E_g^{-9/4}$ [5]. When comparing operation at different wavelengths one should have in mind that besides the weak dependence (dispersion) of the d_{il} elements, which can be estimated from Miller's rule on the basis of the refractive index dispersion, there is much stronger dependence through the coupling constant and the figure of merit can be redefined as FM$^* \sim d^2/(n^3\lambda_1\lambda_2\lambda_3)$. Thus, operation at longer (idler) wavelengths in general means lower conversion efficiency.

The list of NLCs combining a transparency extending into the mid-IR range above ~5 μm (the upper limit of oxide materials) and large-enough birefringence to permit phase-matching over their transparency ranges is not very long. Their FMs are shown in Fig. 2 versus transparency range. As already mentioned, non-oxide NLCs show higher nonlinearity but lower bandgap in comparison to oxides and their refractive index is also higher. Unfortunately there are no ferroelectrics among them to be used for QPM. The binary and ternary birefringent noncentrosymmetric crystals now in use in this spectral region include the chalcopyrite semiconductors $AgGaS_2$ (AGS), $AgGaSe_2$ (AGSe), $ZnGeP_2$ (ZGP) and $CdGeAs_2$ (CGA), the defect chalcopyrite $HgGa_2S_4$ (HGS), GaSe, CdSe, and Tl_3AsSe_3 (TAS) [6]. Some other crystals like proustite (Ag_3AsS_3) and pyrargyrite (Ag_3SbS_3) have already lost their importance because they were completely replaced by the more technological AGS while the growth technology of HgS (mineral) and $InPS_4$ (chemical vapor transport) was never developed [7,8]. The list of the non-oxide birefringent inorganic crystals used in the past will be full if the elemental (unary) Se and Te are added: Their linear losses are, however, so high that at present they could be interesting, in particular Te, only for diagnostic purposes of ultrashort pulses at longer wavelengths [7]. All these mid-IR crystals are uniaxial. All of them have their specific advantages but also some drawbacks: AGS and AGSe have low residual absorption but poor thermal conductivity and anisotropic thermal expansion with different sign, ZGP has excellent nonlinearity and thermal conductivity but multi-phonon and residual absorption limit its transparency from both sides so that pump wavelengths should lie above 2 μm which corresponds to less than 1/3 of its bandgap, CGA possesses extremely high nonlinearity but exhibits also absorption features and low temperatures are required to avoid residual losses, HGS has a high FM but its growth technology is very difficult (several phases exist) and only small sizes are available, GaSe has large nonlinearity and birefringence but it is a soft, cleaving compound, with very low damage threshold, i.e. difficult for polishing and coating, CdSe is transparent up to 18 μm but its birefringence and nonlinearity are quite modest, TAS exhibits rather low losses in its transparency range but its thermal conductivity, as that of Ag_3AsS_3 and Ag_3SbS_3, is extremely low, and finally Te is a unique nonlinear material having in mind its extended wavelength range and superior nonlinear susceptibility but as already mentioned, its applicability is limited by the high linear losses. At present only AGS, AGSe, ZGP, GaSe, CdSe and Te can be considered as commercially available (HGS, LIS, LISe, LGS and LGSe – available from some institutions in limited sizes/quantity). The monoclinic (biaxial) $Sn_2P_2S_6$ is included in Fig. 2 for completeness: it is a relatively well characterized compound possessing ferroelectric properties but a phase transition at 338 K to a centrosymmetric phase makes it impractical [9].

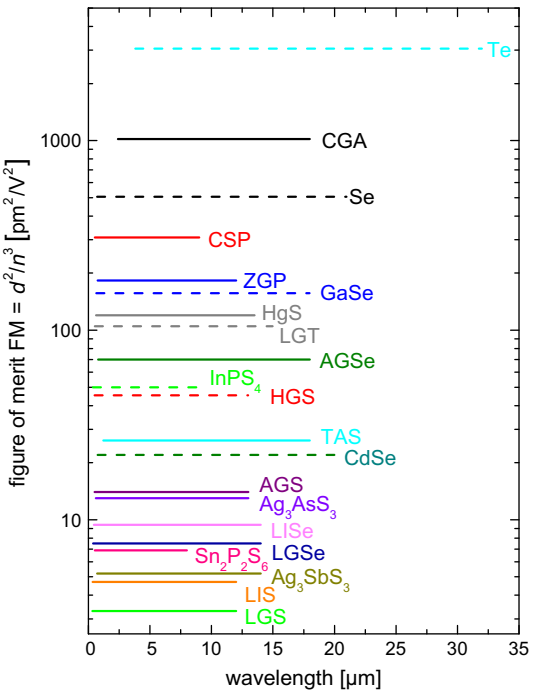

Fig. 2. Nonlinear figure of merit of non-oxide birefringent NLCs versus transparency range. The data on HgS, TAS, and Se is very old and the FM error in this diagram is ±50%. Note that oxide NLCs typically have much lower FM, in the best cases (e.g. $KNbO_3$) reaching ~10 pm^2/V^2.

The above crystals are known for quite a long time, for some of them (e.g. AGS, AGSe, ZGP, CGA) improvement of grown technology, reduction of residual losses, etc. still continue after few decades of development, others were never developed (HgS, $InPS_4$) or abandoned (Ag_3AsS_3 and Ag_3SbS_3) in favor of more promising ones. Improved NLCs are, however, critical for advancing mid-IR coherent source development and especially to increase the conversion efficiency and the output power. Important challenges include also compatibility with powerful 1 μm pump sources (Nd and Yb laser systems) or, in the femtosecond domain, even 0.8 μm (Ti:sapphire laser systems), which means relatively wide bandgap. As already mentioned, this unfortunately contradicts the basic requirement for high nonlinear coefficients. Other desirable properties include low residual losses, high damage threshold, high thermal conductivity and the possibility for NCPM. Problems that occur include the already mentioned TPA (except for the cw regime), the achievable sizes (especially for OPO), the homogeneity of the grown crystals, the surface (chemical) stability, and the damage resistivity of the anti-reflection (AR) coatings necessary when cavities are employed.

Few trends can be observed in the development of new mid-IR crystals in the last decade that are, to a greater part, related to the development of laser pump sources. The first one is in fact a rather old idea of doping or mixing binary or ternary compounds to obtain new, more complex ternary compounds like GaS_xSe_{1-x} [10] or quaternary compounds like $AgIn_xGa_{1-x}S(e)_2$, $Cd_xHg_{1-x}Ga_2S_4$ or $Ag_xGa_xGe_{1-x}S(e)_2$ [11,12]. Adding S to GaSe not only improves the thermo-mechanical properties (the same does In) but increases the bandgap thus helping to avoid TPA at 1064 nm (see Table 2). Mixing AGS(e) or HGS compounds with the isostructural but

Table 2
Summary of important properties of birefringent NLCs that can be pumped at 1064 nm to generate 6.45 μm light: The effective nonlinearity d_{eff} (column 3) is calculated at the corresponding phase-matching angle θ or φ (column 2), the nonlinear tensor components, d_{il}, used for this calculation were derived from the literature (column 6) applying Miller's rule (column 7). The wavelength λ_F (fundamental) at which the nonlinear coefficients have been estimated by SHG is also shown in column 6. For $Sn_2P_2S_6$, d_{eff} is taken directly from the literature [9].

Crystal Point group	Plane	θ/φ [°] (Interaction)	d_{eff} [pm/V]	Thermal conductivity [W/mK]	Band-gap E_g [eV]	Miller's δ [pm/V] or d_{il} [pm/V] @ λ_F for SHG	+Miller's correction [pm/V]
$AgGaS_2$* $\bar{4}2m$		40.50 (oo-e) 45.53 (eo-e)	8.86 13.65	1.4//***c*** 1.5 ⊥***c***	2.70	δ_{36} = 0.12	d_{36} = 13.65
$HgGa_2S_4$* $\bar{4}$		45.87 (oo-e) 51.21 (eo-e)	15.57 21.18	2.49–2.85//***c*** 2.36–2.31 ⊥***c***	2.79	d_{36} = 27.2 @ 1064 nm	d_{36} = 24.56
$Cd_xHg_{1-x}Ga_2S_4$* (θ = 90°, x = 0.55) $\bar{4}$		90.00 (oo-e)	24.94	1.8–1.92//***c*** 1.62–1.81 ⊥***c*** (x = 0.27–0.3)	3.22 (x = 0.55)	d_{36} = 27.2 @ 1064 nm	d_{36} = 24.94
$LiGaS_2$ *mm*2	*xz* *xy*	47.77 (oo-e) 40.36 (eo-e)	4.23 5.50	NA	3.76	d_{31} = 5.8 d_{24} = 5.1 @ 2300 nm	d_{31} = 5.71 d_{24} = 5.21
$LiInS_2$ *mm*2	*xz* *xy*	40.01 (oo-e) 36.37 (eo-e)	4.65 6.77	6.2//***x*** 6.0//***y*** 7.6//***z***	3.57	d_{31} = 7.25 d_{24} = 5.66 @ 2300 nm	d_{31} = 7.23 d_{24} = 5.93
$LiGaSe_2$ *mm*2	*xz* *xy*	51.45 (oo-e) 37.61 (eo-e)	7.82 9.31	NA	3.65	d_{31} = 9.9 d_{24} = 7.7 @ 2300 nm	d_{31} = 10 d_{24} = 8.16
$LiInSe_2$* *mm*2	*xz* *xy*	36.97 (oo-e) 41.62 (eo-e)	7.26 10.57	4.7–4.5//***x*** 4.7–4.8//***y*** 5.5–5.8//***z***	2.86	d_{31} = 11.78 d_{24} = 8.17 @ 2300 nm	d_{31} = 12.08 d_{24} = 8.65
$LiGaTe_2$ $\bar{4}2m$		36.38 (ee-o) 40.05 (oe-o)	46.20 31.12	NA	2.41	d_{36} = 43 @ 4600 nm	d_{36} = 48.37
$BaGa_4S_7$ *mm*2	*xz*	4.64 (oo-e)	NA	NA	3.54	NA	NA
$BaGa_4Se_7$ *m*	*yz* *xz* *xz*	30.30 (oe-o) 50.68 (ee-o) 54.38 (oe-o)	NA	NA	2.64	NA	NA
$InPS_4$ $\bar{4}$		38.80 (ee-o) 42.67 (oe-o)	34.40 23.87 @ optimum φ	NA	3.2	δ_{31} = 0.39 δ_{36} = 0.30	d_{31} = 27.87 d_{36} = 21.53
$Sn_2P_2S_6$ *m*		(ss-f) (fs-f)	≈4 ≈2	0.4–0.55	2.35	...	...
$GaS_{0.4}Se_{0.6}$ $\bar{6}2m$		22.31 (oo-e) 24.67 (eo-e)	45.80 40.88	1.3//***c*** 10 ⊥***c***	2.4	d_{22} = 44.1 @ 4.65 μm	d_{22} = 49.51
$CdSiP_2$* $\bar{4}2m$		80.46 (oo-e)	90.99	13.6	2.2–2.45	d_{36} = 84.5 @ 4.56 μm	d_{36} = 92.27
$AgGaGeS_4$ *mm*2	*xz* *xy*	53.99 (oo-e) 35.74 (oo-e)	3.32 5.43	0.399	3.0	d_{32} = 6.2 d_{31} = 10.2 @ 1064 nm	d_{32} = 5.65 d_{31} = 9.30
Ag_3AsS_3* 3*m*		22.04 (oo-e) 24.01 (eo-e) 65.63 (oe-e)	22.89 16.44 3.35	0.113//***c***, 0.092 ⊥***c***	2.2	d_{31} = 10.4 d_{22} = 16.6 @ 10.6 μm	d_{31} = 12.34 d_{22} = 19.70
Ag_3SbS_3 3*m*		47.14 (oo-e) 52.84 (eo-e)	14.34 3.80	~0.1//***c***, ~0.09 ⊥***c***	2.2	d_{31} = 7.8 d_{22} = 8.2 @ 10.6 μm	d_{31} = 9.90 d_{22} = 10.41

* Crystals for which OPO with ~1 μm pump wavelength has been already demonstrated.

low-birefringence $AgInS(e)_2$ or $CdGa_2S_4$ compounds, respectively, allows NCPM configurations with maximized effective nonlinearity to be achieved. In decreases the bandgap and slightly improves the nonlinearity of AGS(e) crystals while Cd has the opposite effect on HGS. Indeed, the latter enabled pumping of $Cd_xHg_{1-x}Ga_2S_4$ at 1064 nm (Table 2). Mixing AGS(e) compounds with $GeS(e)_2$ produces new orthorhombic (biaxial) structure, different from the chalcopyrite structure of AGS(e), and the resulting quaternary compounds (see Fig. 3) exhibit increased band-gap and improved damage resistivity. $CdGe(As_{1-x}P_x)_2$ and $AgGa(Se_{1-x}S_x)_2$ have also been studied, they are quaternary compounds which are isostructural to their parent ternary compounds and the mixing permits to engineer the bandgap, the nonlinearity and the birefringence (phase-matching properties).

The main problem with such mixed crystals is the varying composition along the grown boule and also in radial direction. It seems that it is easier to achieve constant composition when the new mixed compound exhibits different crystallographic structure, e.g. $Ag_xGa_xGe_{1-x}S(e)_2$ and GaS_xSe_{1-x} (Figs. 3 and 4). Nevertheless, the problem seems to have no real solution and the interest in such crystals seems to decline. An elegant way to utilize the variation of the composition for tuning of an OPO, has been demonstrated with $Cd_xHg_{1-x}Ga_2S_4$ [11] and such an active element is shown in the upper part of Fig. 3.

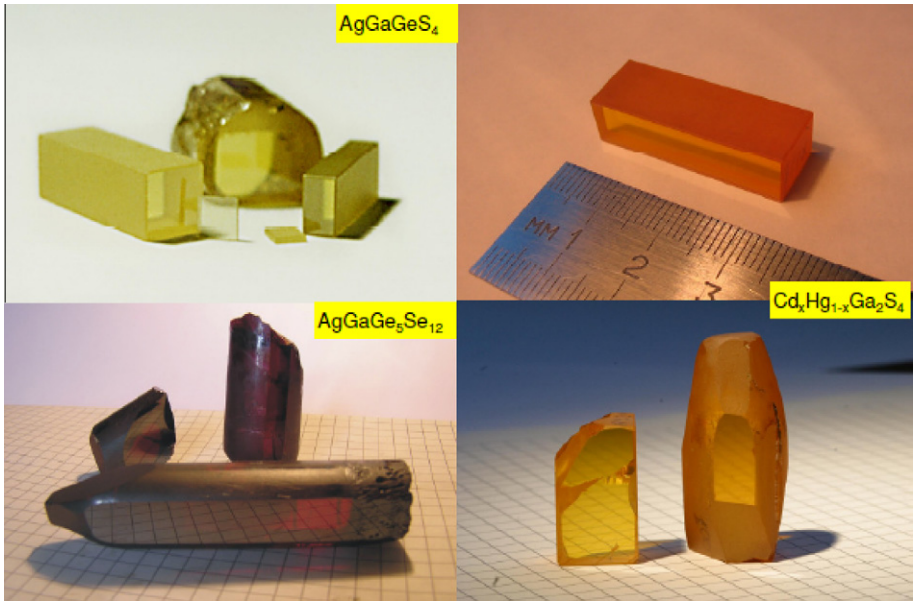

Fig. 3. Crystals of quaternary $AgGaGeS_4$ and $AgGaGe_5Se_{12}$ (left), and $Cd_xHg_{1-x}Ga_2S_4$ (right) grown by the Bridgman–Stockbarger method [courtesy of V. Badikov, Kuban State University].

Fig. 4. Layered crystal of $GaS_{0.4}Se_{0.6}$: the maximum S-content preserving the noncentrosymmetric structure of the mixed compound (the transmission in the visible is obviously improved in comparison with GaSe), cube and prism made of CSP to measure thermo-mechanical and dispersive properties, ingots of orthorhombic Li-compounds after annealing, and first grown samples of LGT [courtesy of V. Panyutin (Kuban State University), top-left, P. Schunemann (BAE Systems), top-right, and L. Isaenko and A. Yelisseyev (Institute of Geology and Mineralogy), bottom pictures].

A second trend in the development of new mid-IR NLCs is to trade a property which is available in abundance, such as the high nonlinearity, for properties which favor low loss and damage threshold. The best example here is the development of the chalcopyrite $CdSiP_2$ (CSP) by P. Schunemann at BAE Systems [13]. In this case moving to a wider bandgap among the chalcopyrite compounds of the II–IV–V_2 class is associated with higher hardness and thermal conductivity but also with higher melting point and vapor pressures, and more difficult crystal growth. Nevertheless, in this case the result was impressive: CSP turned out to have nonlinearity exceeding that of ZGP but in contrast to ZGP it is phase-matchable for 1064 nm (and also 1.5 μm) pumping without TPA and the only crystal that can offer NCPM for a 1064 nm pumped OPO with idler output in the 6 μm range. In fact, the nonlinear coefficient of CSP is not only the highest among all NLCs that can be pumped at 1064 nm (Table 2), it is the highest of a new inorganic crystal in almost 40 years. As can be seen from Fig. 2, CSP has a very high FM but multiphonon absorption limits its practical wavelength range to ~6.5 μm.

In the last decade, considerable progress has been made also with four orthorhombic (biaxial) wide band-gap ternary chalcogenides, $LiInS_2$ (LIS), $LiInSe_2$ (LISe), $LiGaS_2$ (LGS), and $LiGaSe_2$ (LGSe),

whose growth technology was improved to such an extent that it was possible to perform extensive characterization and even realize some applications [14–17]. Moreover, their attractive features already stimulated the study of further crystals belonging to the same class, like $LiGaTe_2$ (LGT) which is now under development [18]. Li-compounds exhibit wider band-gap than their Ag-analogs (AGS, AGSe, etc.). Their wurtzite type structure (except for LGT) leads to better thermo-mechanical and damage properties. However, the nonlinearity of the Li-compounds is lower than in their Ag-analogs and the FMs are among the lowest (Fig. 2), comparable to some oxide NLCs. Nevertheless, LGS, LIS, and LGSe are the only known non-oxide materials that can be pumped by femtosecond Ti:sapphire laser systems operating near 800 nm without TPA. Two related compounds, $BaGa_4S_7$ (BGS) and $BaGa_4Se_7$ (BGSe) could be recently added to this group (Table 2) but the nonlinearities of these crystals are still unknown [19]. LGT in turn shows extremely wide bandgap for a telluride compound and its FM is quite high (Fig. 2). In contrast to $AgGaTe_2$, LGT is sufficiently birefringent and can be even pumped at 1064 nm (Table 2). However, the surface of this material is chemically unstable. Table 2 summarizes the properties of all non-oxide NLCs that can be phase-matched by birefringence at a pump wavelength of 1064 nm (Nd:YAG laser) without exhibiting TPA. For proper comparison, a definite idler wavelength (6.45 μm – target wavelength for medical applications) is selected.

The third trend is the manufacturing of QPM orientation patterned structures with highly nonlinear but isotropic semiconductors, e.g. GaAs which has a mature technology [20], as an alternative to patterned electric field poling which is applicable only to ferroelectric oxide crystals. This has few essential advantages: (i) large nonlinear coefficient for QPM ($d_{eff} \sim 60$ pm/V), (ii) NCPM with long interaction lengths (especially important for cw operation) reaching e.g. 70 mm, (iii) low absorption losses ($\leqslant 0.02$ cm^{-1}), (iii) wide transparency range (1–18 μm), (iv) high thermal conductivity (46 W/mK). The chief obstacle to achieving QPM in GaAs and similar cubic crystals (GaP, InAs, InP, InSb, ZnSe, etc.) is the process of creating a modulated structure from a non-ferroelectric material. While previous attempts relied on diffusion bonding of stacks, the current approach is based on orientation patterned crystal growth (orientation-patterned GaAs, or OPGaAs). Diffusion bonding provides large apertures but the period is set by polishing, the fabrication process is serial, the sample lengths are limited and short periods scale poorly. The orientation-patterned crystal growth requires a template for the growth of the structure, Fig. 5. Its advantages include the possibility to set the period by photolithography, the parallel fabrication process, the long sample lengths that can be achieved and the short periods that are equally possible. The basic limitation is the small aperture (thickness) that can be obtained with sufficient quality of the structure (Fig. 6). It is expected, however, that gratings of few millimeter thickness will be available soon on the basis of OPGaAs. The high growth rates (>150 μm/h) are promising for bulk devices.

3. Down-conversion to the mid-IR using non-oxide nonlinear materials

3.1. Down-conversion of cw radiation

Parametric down-conversion in the cw regime offers ultra-narrow spectral linewidths (down to the 100 kHz range) with single-frequency operation possible, better frequency stability, and continuous scan options at the expense, however, of lower conversion efficiency. Unfortunately, due to the difficulties already mentioned, cw OPO operation above 3 μm has not been demonstrated with a non-oxide NLC, yet. The only cw OPO that operated with a non-oxide crystal (AGS) generated an idler at 2535 nm [21]. Essential for this achievement was the use of NCPM with a 15 mm long AGS crystal (type-I, oo-e phase-matching) and tight focusing in the 30 mm long cavity consisting of two highly-reflecting RC = −50 mm concave mirrors. It was the NCPM condition (operation at $\theta = 90°$) that required the use of rather short pump wavelength (845 nm, from a single-mode, grating-tuned extended cavity GaAlAs diode laser with a typical short-term linewidth of ~100 kHz and a tapered GaAlAs amplifier) and the resulting signal and idler wavelengths were near 1267 and 2535 nm, respectively. The triple-band AR-coated AGS crystal had ~1%/cm absorption loss at the pump wavelength and ~0.5%/cm loss at the signal. The (external) pump threshold power for this doubly-resonant OPO with weak pump enhancement (weakly triply resonant OPO) was in the 60–70 mW range. The output power saturated at ~2 mW from each cavity side which corresponds to ~2% efficiency for 200 mW of pump power but only 5% of the single-mode output power was in the idler wave because of the much smaller residual transmission of the mirrors at 2535 nm. Further studies of this OPO using different crystals and cavity arrangements identified strong thermal effects induced by the residual absorption as the main

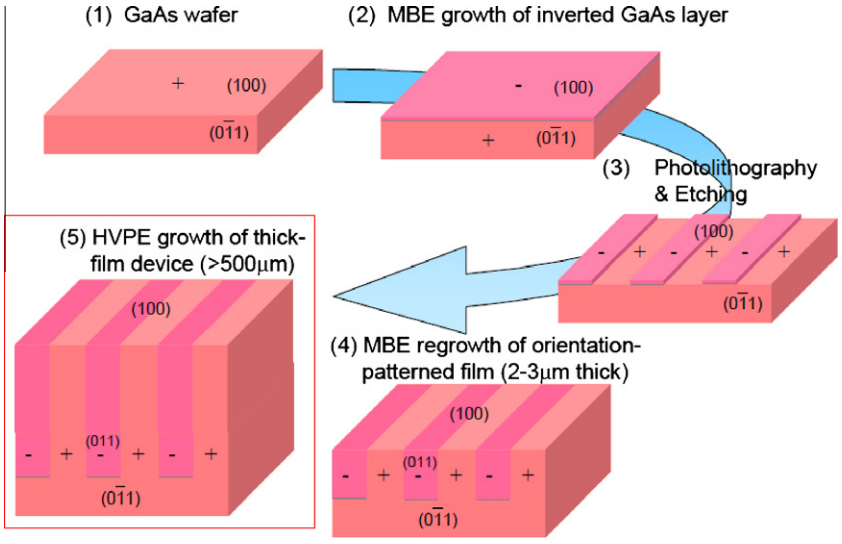

Fig. 5. All-epitaxial growth of OPGaAs (developed at Stanford University and scaled to 3″ at BAE Systems).

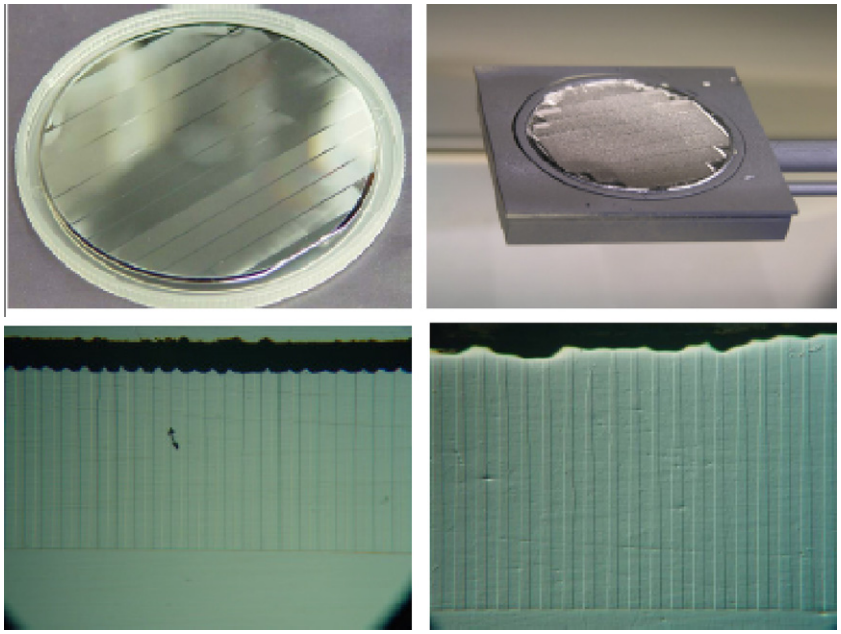

Fig. 6. (Top, left) 3″ MBE (Molecular Beam Epitaxy) manufactured template for multiple grating OPGaAs, (top, right) HVPE (Hydride Vapor Phase Epitaxy) grown multi-grating OPGaAs as removed from reactor, (bottom, left) 60.6-μm period, 605-μm thick OPGaAs, and (bottom, right) 135-μm period, 1.68-mm thick OPGaAs [courtesy of P. Schunemann, BAE Systems].

limiting factor and confirmed that low intracavity losses (⩽1% per round trip) are desirable to balance the weak cw parametric gain. Of course, materials with better thermal conductivity, see Table 2, could be also a solution for the future.

DFG can be realized in non-oxide NLCs with various single frequency pump sources but the efficiency is extremely low. In general at least one of the input waves has to be tunable in order to obtain idler tunability but if NCPM is utilized and temperature tuning is not feasible, both input waves have to be tuned. Tight focusing and long crystals are as essential as in OPOs. In the 1970-ies, angle tuned crystals of AGSe and CGA were used for mixing CO and CO_2 lasers, and Te for mixing of spin flip Raman and CO_2 lasers, but from the beginning of the 1990-is AGS and especially type-I NCPM (with crystal lengths up to 45 mm) became the main choice. At first, combinations of two dye lasers or dye and Ti:sapphire lasers were used for mixing because typically NCPM requires relatively short input wavelengths (600–1100 nm) but later all-solid-state systems were the lasers of choice. Thus, diode lasers or amplified diode lasers were mixed with Ti:sapphire lasers or two laser diodes were mixed. If angle tuning has to be applied because the NCPM condition is not fulfilled for the available sources, type-II eo-e phase-matching in AGS is preferable with its higher d_{eff}. Fig. 7a shows the simple scheme of mixing two 500 mW amplified, tunable single-frequency (short-term linewidth <200 kHz) laser diodes in such a 10-mm long AGS [22].

Tuning of the idler was possible from 6.8 to 12.5 μm and this is the longest wavelength achieved with AGS. The maximum power obtained in the mid-IR was 1.3 μW at 8 μm and the maximum internal conversion efficiency reached 15.6 $\mu W/W^2$. Computer controlled scans were possible over >2 cm^{-1} and the spectral resolution, having in mind the frequency jitter specifications of the laser diodes, was estimated to be <4 MHz (<0.00015 cm^{-1}).

Extension to longer input wavelengths (both >1.1 μm) when mixing two laser diodes was demonstrated by type-I AGSe instead of AGS but the actual coverage of longer idler wavelengths (up to 19 μm) was achieved with GaSe using two Ti:sapphire lasers [23]. Other crystals employed for DFG with Ti:sapphire lasers were LIS and LISe. As with GaSe, angle tuning had to be used with them but they did not show any advantages over AGS. On the other hand, one possibility to improve the conversion efficiency in DFG is the use of cavity enhancement, realized so far for the signal wave (from a Nd:YAG laser) when mixed with a diode laser in a short AGS crystal or for both, signal and pump waves, under critical type-I phase-matching in AGS, when mixing (amplified) laser diodes, also with

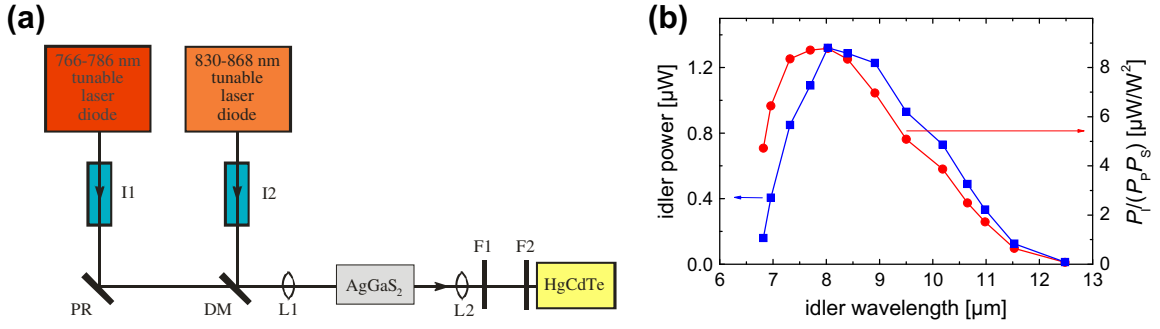

Fig. 7. (a) Mixing of single frequency laser diodes in type-II (eo-e) AGS: I1, I2, optical isolators, PR, polarization rotation in off-plane 90° bending, DM, dichroic mirror, L, lenses, F, long-pass filters, HgCdTe, N_2 cooled detector. (b) Idler power and external conversion efficiency versus idler wavelength.

AGS. Intracavity DFG in a AGS crystal positioned in the cavity of a Nd:YAG laser (signal) and pumped by a tunable Ti:sapphire laser was also demonstrated, with a tuning range from 3.1 to 4.4 μm.

Summarizing, cw DFG with non-oxide NLCs produces mid-IR powers between 0.01 and 1 μW when diode lasers are mixed and up to 50 μW (albeit near 4.3 μm [24]) when Ti:sapphire lasers or diode amplifiers are involved. The intracavity DFG scheme produced even 300 μW, however, near 3.2 μm [25]. The spectral resolution typically achieved is in the 1–100 MHz range. One of the problems observed with AGS is the low surface damage threshold with cw radiation (as low as 3 kW/cm^2). A major limitation for AGS or AGSe remains the fact that temperature tuning or QPM are not feasible. In fact, this type of narrow-band mid-IR sources seems to lose its importance. On the one hand, in the wavelength range up to 5 μm similar devices based on oxide materials (e.g. periodically-poled $LiNbO_3$ (PPLN), periodically poled $KTiOPO_3$ (PPKTP) and similar) provide 1–2 orders of magnitude higher (∼mW) DFG power while OPOs based on such materials generate even powers on the watt level in the cw regime. On the other hand, there is strong competition also from alternative narrow-band and tunable mid-IR quantum-cascade lasers (QCLs). The situation could probably change only due to the introduction of OPGaAs. The NCPM through QPM relaxes the constraints on the input wavelengths which are then normally above 1250 nm and it is also possible to use unpolarized laser sources (from fibers) because of the cubic symmetry of GaAs. In the first such experiment, laser diodes (one of them amplified in Er-fiber) were used with a 0.5 thick, 19-mm long OPGaAs. The system was improved later, with two laser diodes amplified in Er- and Pr-fiber amplifiers before mixing them in a similar OPGaAs crystal, tuning in the 7–9 μm range by both pump wavelength and temperature. Finally, output powers as high as 0.5 mW were obtained with similar tuning in the 7.6–8.2 μm range [26]. In this case, Er-fiber amplifier seeded by a laser diode and Tm-fiber laser-amplifier served as high power sources to be mixed in a 0.45 mm thick, 33 mm long OPGaAs crystal.

3.2. Down-conversion of nanosecond pulses

OPOs are typically pumped either with ∼10 ns long pulses corresponding to repetition rates of the order of 10 Hz, from flash-lamp pumped lasers with electro-optic Q-switching, in order to achieve maximum output energies, or with ∼100 ns at typically 1–50 kHz repetition rate from diode-pumped laser systems with acousto-optic Q-switching, to achieve maximum average output powers. However, the pump pulse duration depends on the type of pump source used which is sometimes also gain-switched. The shortest wavelength at which nanosecond OPOs based on non-oxide materials can be pumped without the onset of TPA is about 1 μm, corresponding to Nd- or Yb-laser systems. This is simultaneously a very desirable pump wavelength range because exactly such Nd-laser based pump systems are most advanced at present and offer power scaling through diode-pumping. However, at the same time, as already mentioned, TPA is a more stringent limitation on the choice of non-oxide NLCs at such wavelengths.

The non-oxide materials already employed in nanosecond OPOs pumped in the 1 μm range are indicated in Table 2. In the first demonstrations from the beginning of the 1970-ies, Ag_3AsS_3 was the crystal of choice and in fact it was only the very first report [27] in which 2 kHz repetition rate was used – cumulative surface damage problems made it necessary to further operate such systems mostly at 10 Hz. Also, only in these early attempts was it necessary to employ doubly-resonant OPOs in order to reach the threshold, further realizations were only with singly resonant OPOs but in most of the cases with retroreflection of the pump (double pump pass) in order to better deplete it. The pump pulse duration of the Nd-lasers used for pumping was in the 10–30 ns range and in most of the cases the pump was in the TEM_{00} fundamental mode but not single-frequency. AGS remains the most widely studied such NLC at 1064 nm pump. The essential advantage of using HGS instead of AGS is its much higher FM, Fig. 2, which makes it possible to use active elements as short as 6 mm while for AGS the crystal length as a rule was 20 mm. HGS produced also the highest output idler energy, 3.3 mJ, and average power, 67 mW at 20 Hz, near 4 μm [28]. However, it should be noted that all AGS and HGS OPOs reported, generated idler wavelengths not exceeding 5.3 μm, with one exception, the impressive tunability from 3.9 to 11.3 μm (∼0.37 mJ maximum energy at 6 μm), achieved in [29] with AGS at 10 Hz. The solid solution $Cd_xHg_{1-x}Ga_2S_4$ on the other hand enabled for the first time NCPM in a 1-μm pumped OPO which is impossible in AGS or HGS at such long pump wavelengths [30]. The 11-mm thick AR-coated for the signal wave active element shown in Fig. 3 was studied in a 3 cm long cavity, with 22 ns long pump pulses. The varying composition from $x = 0.21$ to 0.25 allowed smooth tuning of the idler wavelength from 2.85 to 3.27 μm by translation along the c-axis over a range extending from $z = 0$ to 28 mm (Fig. 8b). The maximum conversion efficiency of 3.8% at the idler wavelength of 3.03 μm corresponds to a slope of 6.6% (Fig. 8a). The asymmetry in the spatial distribution (insets Fig. 8a) was likely due to the different angular acceptance with respect to θ and φ. The measured energy conversion efficiency and estimated slopes are also shown in Fig. 8b in dependence on the position in the crystal. Their scatter indicates rather smooth variation of the crystal composition except for one of the end positions.

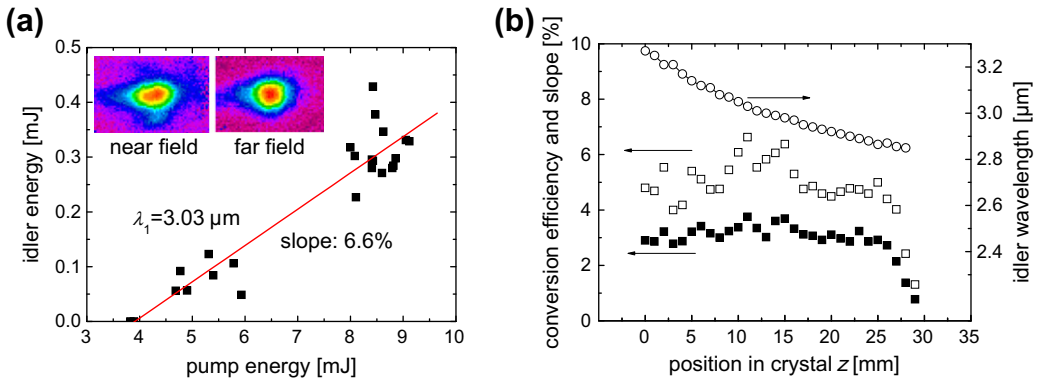

Fig. 8. (a) Idler energy versus pump energy of the tunable $Cd_xHg_{1-x}Ga_2S_4$-OPO for a crystal position corresponding to $z = 11$ mm (measured along the 30.6 mm dimension), see (b). The insets show the spatial distribution of the idler intensity. (b) Idler wavelength (circles), conversion efficiency (full squares) and slope efficiency (open squares) versus position z in the crystal.

Recently, nanosecond OPOs pumped by Nd:YAG lasers were demonstrated also with CSP [31,32] and LISe [16]. CSP is the first NLC which, without being a solid solution, enabled NCPM at 1064 nm in type-I (oo-e) configuration. With an 8-mm long crystal the pump threshold of the CSP OPO pumped by 14 ns pulses was about 1.8 mJ and the maximum idler energy measured at 10 Hz repetition rate was 0.47 mJ at ~6.2 μm, at an incident pump energy of 21.4 mJ, Fig. 9 [31]. This gives a conversion efficiency of 2.2% for the idler alone or a quantum conversion efficiency of ~12.8%. Only slightly lower output powers were observed at 20 Hz which can be attributed to the residual crystal absorption at the pump wavelength. The maximum average output power (idler only), reached in this case, was 9.1 mW. The output energy level achieved with this very first sample of CSP already exceeds the best result previously reported at such long wavelengths with ~1 μm pumped OPOs, the above mentioned 372 μJ at 6 μm obtained with AGS [29]. Moreover, the input/output characteristics in Fig. 9b show no saturation, in contrast to [29], which means that power scaling can be expected even without increasing the pump beam diameter.

Moreover, CSP enabled two further innovations [32]: the exceptionally high FM (Fig. 2) permits the use of rather short crystal/cavity lengths, and consequently to pump with relatively short pump pulses, achieving, for the first time with any OPO, sub-nanosecond signal and idler pulse durations, (ii) the good thermo-mechanical properties (Table 2) enabled for the first time stable and long term 1-kHz repetition rate operation with a non-oxide nonlinear material pumped at 1064 nm. The pump source in this case provided incident energy up to 1.15 mJ at 1 ns pulse duration at 1064 nm. The OPO threshold was 120 μJ of pump energy and the maximum idler energy achieved was 24 μJ at 6.125 μm which translates into an average power of 24 mW. In contrast to the related ZGP, temperature tuning is feasible for CSP providing an extension of the non-critical tuning range to the long wavelength transmission limit, which covers the essential for medical applications spectral region near 6.45 μm, Fig. 9c. The output idler energy is almost constant when changing the temperature, slightly decreasing above 6.4 μm, partially due to the idler absorption. The signal pulse duration amounted to 0.75 ns, shorter, as expected, than the pump pulse duration and the idler pulse duration should be similar to that of the signal [32]. Moreover, the CSP crystal seems to be more damage resistant at such short pump pulse durations.

As already mentioned, the only disadvantage of CSP seems its 6.5 μm upper wavelength limit. With a similar set-up as the one shown in Fig. 9a, and the same 14 ns pump source, it was possible to achieve broadly tunable operation, from 4.7 to 8.7 μm (Fig. 10b), with LISe (type-II eo-e angle phase-matching), a crystal exhibiting better thermo-mechanical and damage resistivity properties than AGS, Table 2, [16]. The maximum idler energy reached 282 μJ at 6.514 μm (Fig. 10a), at a repetition rate of 100 Hz. The average idler power of ~28 mW is the highest ever achieved with a 1-μm pumped OPO in this spectral range and the improvement with respect to AGS (operating at 10 Hz, restricted by cumulative damage) was 7-fold.

Moving to longer pump wavelengths, AGSe was pumped by 1.32–1.34 μm Nd-lasers, also in NCPM but angle tuning was then limited to 6.7–6.9 μm. This pump wavelength is also slightly too short and TPA occurs. Er:YLF laser operating near 1.73 μm was a much better alternative for AGSe and indeed very high idler energies were achieved with such an OPO albeit at very low repetition rates. Similarly, a CdSe based OPO was pumped at 1.833 μm by a Nd:YAG laser with the idler between 9.8 and 10.4 μm, tuned by angle tilt near the NCPM point: Also in this crystal, broader tuning would require longer pump wavelengths.

Pumping OPOs near 2 μm has produced the best results so far in terms of output energy and/or power mainly because an excellent material, ZGP (Fig. 2), is available for such pump wavelengths. Spatial walk-off compensation and two crystals can be used because at

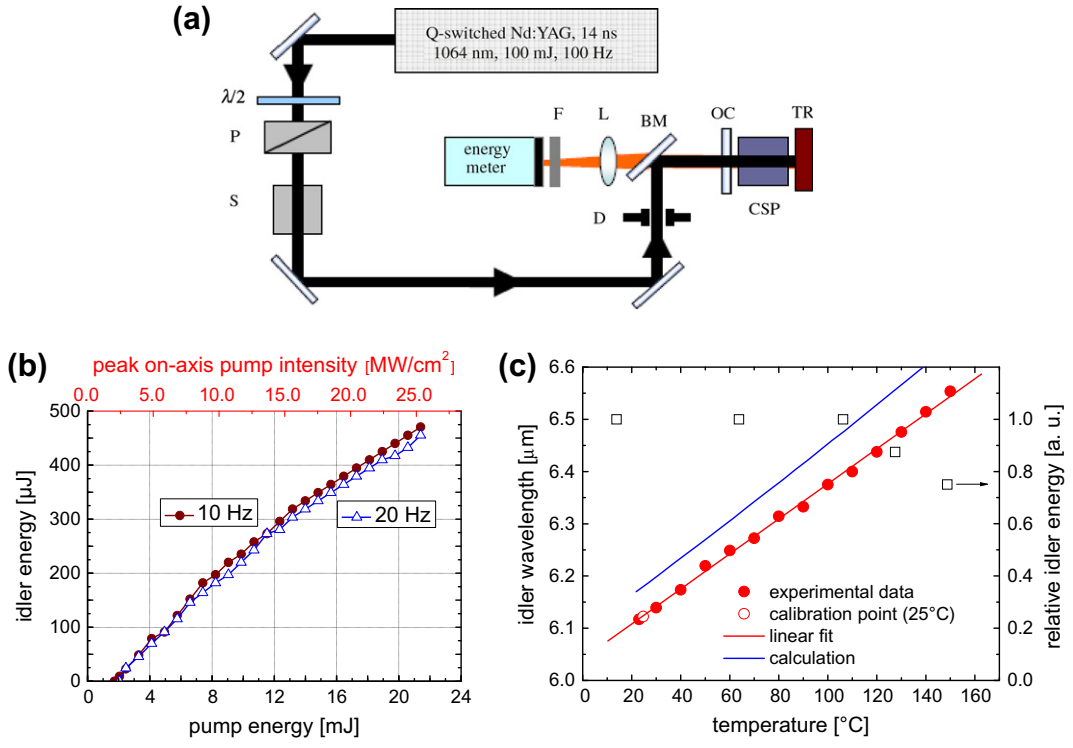

Fig. 9. (a) Experimental set-up of the CSP OPO: λ/2, half-wave plate, P, polarizer, S, mechanical shutter, F, cut-on filter, L, MgF_2 lens, D, diaphragm, BM, bending mirror, OC, output coupler, TR, total reflector. (b) Idler energy versus incident pump energy for two repetition rates in the case of 14 ns long pump pulses. (c) Temperature tuning in NCPM with a similar set-up and 9.5-mm long CSP crystal pumped by 1 ns, 1064 nm pulses at 1 kHz.

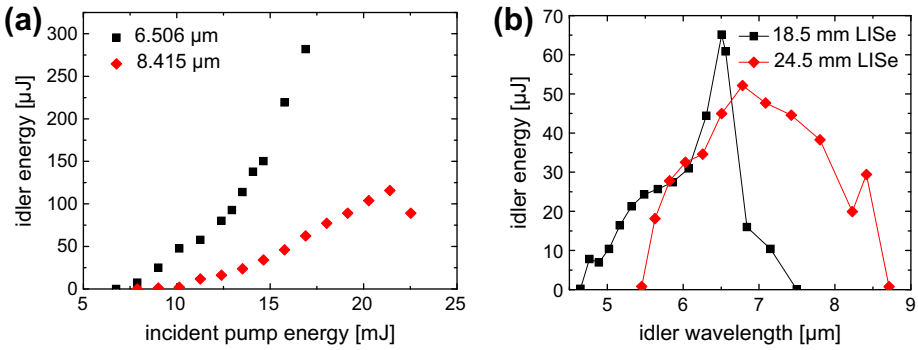

Fig. 10. (a) Output idler energy with 17.6-mm long (black squares) and 24.5-mm long (red diamonds, the last point denotes surface damage) LISe crystals with different cuts, at normal incidence, versus incident pump energy at 1064 nm. (b) Tuning OPO curves recorded for the two LISe samples at fixed pump energy. (For interpretation of the references to colour in this figure legend, the reader is referred to the web version of this article.)

such pump wavelengths type-I (ee-o) phase-matching in ZGP is critical. Ho-lasers were initially preferred because they emit slightly above 2 μm where the residual (defect) absorption of ZGP is lower but diode-pumping of such lasers was developed only very recently and typically they are pumped by Tm bulk or fiber lasers or rely on Tm-codoping as a sensitizer. However, with the improvement of the crystal quality, it became possible to directly pump ZGP OPOs with Tm-lasers.

The high damage threshold and good thermal conductivity of ZGP are compatible with both high energy operation at low repetition rates and high average power operation at kilohertz repetition rates. Diode pumped Tm:Ho:YLF, Tm:Ho:LLF, and Tm:Ho:$GdVO_4$ lasers and amplifiers (typically requiring cooling) or lamp-pumped Cr:Tm:Ho:YAG (at 5 Hz) have been used for pumping. Pumping a singly resonant ZGP OPO with a low repetition rate (6 Hz) diode-pumped Tm:Ho:LLF laser system produced idler energies as high as 17.3 mJ at 4.8 μm (27.5% pump conversion efficiency to idler and 70% total slope efficiency) [33]. The OPO was tunable up to 10.1 μm where ZGP already absorbs. Employing a Q-switched Ho:YAG (2.09 mm) laser pumped by two diode-pumped Tm:YLF lasers enabled 10.6 W mid-IR power not far from degeneracy (3.9 and 4.6 μm in a doubly resonant configuration) [34] and 0.96 W at 8.08 μm [35], in both cases at 10 kHz repetition rate.

At present the most promising concept for power scaling seems Tm-fiber laser pumping of Q-switched Ho:YAG or Ho:YLF lasers. With this concept, 30 W of average power have been extracted from a ZGP OPO (signal plus idler, between 3 and 5 μm), pumped by 53 W Ho:YAG laser (56% total conversion efficiency and 66% slope efficiency) at 10 kHz [36], and 0.95 W near 8 μm (10.7% conversion efficiency to idler) at 20 kHz [37]. The power level achieved in [37] at the longest idler wavelength of 9.8 μm was ~0.2 W. Combinations of OPO and OPA are suitable for power scaling at lower repetition rates: 31 mJ signal output at 3.4 μm was obtained from such a ZGP OPA operating with 11 mJ seed signal from the OPO [38], based on the Rotating-Image Singly-resonant Twisted-Rect-Angle (RISTRA) concept which improves the spatial quality and helps avoid damage. This system was pumped by a Tm-fiber laser pumped master-oscillator power-amplifier Ho:YLF laser system at 100 Hz.

Direct pumping with Tm:$YAlO_3$ laser at 1.99 μm has also been demonstrated for a ZGP OPO in the doubly resonant configuration, yielding 3 W of total (signal plus idler in the 3–5 μm range) output power at 10 kHz [39]. Direct pumping has been realized also with a combination of a gain-switched Tm-fiber laser and fiber amplifier (at 1.995 μm) and the doubly resonant ZGP OPO produced ~0.66 W of average power (signal plus idler) at 30 kHz in the same spectral region, not far from degeneracy [40].

AGSe was also pumped by Ho:YLF or Tm:Ho:YLF lasers but its performance was inferior to that of ZGP, not only because of the lower FM (Fig. 2) but also because of its low thermal conductivity (Table 2). More recently, slope efficiencies comparable to those achieved with ZGP, have been demonstrated with an OPGaAs based doubly-resonant OPO pumped by a Tm-fiber laser pumped Q-switched Ho:YAG laser [41]. Up to 2.85 W of average power (signal plus idler at 3–5 μm) were obtained at 20 kHz with a 0.45 mm thick OPGaAs. CSP has also shown promising performance when pumped at 1.99 μm by a Tm:$YAlO_3$ laser due to its very low absorption at this pump wavelength and high FM (Fig. 2).

At yet longer wavelengths, Q-switched Dy^{2+}:CaF_2 lasers at 2.36 μm (1 Hz repetition rate) have been used to pump CdSe, achieving tunability between 7.88 and 13.7 μm [42], with the short idler wavelength limit in the NCPM configuration. Better utilization of NCPM with this crystal was possible through the discretely tunable (2.7–3 μm) HF laser. With a HF oscillator-amplifier system at 2.87 μm, the CdSe OPO showed angle tuning from 14.1 to 16.4 μm [43]. CdSe and ZGP OPOs (both type-II, critical) were pumped also at 2.79 μm by a 10 Hz flashlamp-pumped Cr:Er:YSGG laser [44] and CdSe showed idler tuning from 8.4 to 12.3 μm with a maximum energy of 2.4 mJ at 9 μm and a total (signal plus idler) slope efficiency of 59%. With a similar pump laser, a 10 Hz singly resonant ZGP OPO yielded idler tuning up to 12.4 μm with an energy of 1 mJ at 8.1 μm which corresponds to 12.8% pump-to-idler conversion efficiency [45]. Finally, a tunable (2.1–2.9 μm) gain-switched Cr^{2+}:ZnSe laser, pumped by a Q-switched Tm:$YAlO_3$ laser, was also employed for pumping a ZGP OPO [46]. This is compatible with NCPM for type-II (oe-o) interaction in ZGP. Slope efficiency of 53% (signal at 4.7 μm plus idler at 5.6 μm) was achieved pumping at 2.55 μm at 1 kHz repetition rate.

Nanosecond OPOs based on non-oxide NLCs can be pumped, however, also in cascaded schemes (tandem OPO), in which the first stage OPO is based on an oxide material and serves basically to shift the wavelength of Nd-laser based systems to 1.5–3.7 μm. Tuning of the pump for the second stage offers the possibility of NCPM, e.g. for type-II ZGP at longer pump wavelengths – which is associated also narrow linewidths. Degenerate or near-degenerate operation of the first stage enables pumping by both signal and idler of the second stage. First stage $LiNbO_3$ or KTP based OPOs have been used to pump AGSe. With a 5 Hz KTP-OPO used as a pump, AGSe OPO idler tunability from 6 to 14 μm was achieved with >1 mJ at 9 μm [47].

For ZGP OPOs, $LiNbO_3$, PPLN, KTA, KTP and PPKTP have been used in the first stage. Few methods were developed to utilize both the signal and idler from the first stage. First of all, operating the KTP type-II OPO at degeneracy (2.13 μm) the signal and idler can be separated by a polarizer to pump two separate ZGP OPOs

[48]: a total power of 24 W at 20 kHz was obtained by such a system (signal at 3.7–4.1 μm plus idler at 4.4–4.8 μm). A wavelength-dependent polarization rotator has been also developed to transform the orthogonal polarizations at the KTP-OPO output into a common polarization state when operating near-degeneracy [49]: Such a single ZGP-OPO produced a total output power of 5.5 W at 15 kHz repetition rate, however, with pumping at two slightly different wavelengths this power was distributed among two couples of signal and idler, at 3.5, 4.3, 4.6 and 5.5 μm. PPKTP based OPOs provide single output polarization but to reduce the output linewidth, volume Bragg gratings were employed which ensured singly resonant operation near degeneracy of the first OPO stage [50]: Both signal and idler were used then to pump the ZGP OPO which produced 3.2 W (signal plus idler between 3.7 and 5 μm) of average power at 20 kHz, in this case the spectra of the two pairs had almost merged. Finally, the orthogonal output polarizations of the near-degenerate KTP OPO were used to pump separately a ZGP OPO and a ZGP OPA seeded by both signal and idler from the ZGP OPO [51]: This resulted in a total (signal plus idler between 3.8 and 4.8 μm) conversion efficiency of 14% with respect to the 1064 nm pump.

The use of NCPM in type-II ZGP OPO pumped by the idler of a PPLN OPO (tunable between 2.3 and 3.7 μm) enabled a second-stage OPO pump threshold as low as 2 μJ [52]: This system operating at 1 kHz provided also the widest tunability for a tandem OPO, extending from 3.7 to 10.2 μm (signal and idler of the ZGP OPO). Tandem OPOs can be realized also by pumping the ZGP stage intracavity with respect to the KTP OPO [53]: This enabled tuning from 2.7 to 8 μm and the overall slope efficiency (signal plus idler with respect to the 1064 nm pump) reached 35%.

Finally, OPGaAs with its intrinsic NCPM directly profits from the tunable nature of the pump in tandem OPO configurations: With a 0.5 mm thick, 11 mm long OPGaAs, tuning either the pump wavelength from the first stage PPLN OPO between 1.8 and 2 μm, or the OPGaAs temperature, a mid-IR tuning range of 2.28–9.14 μm was achieved with a single grating period [54]: The OPGaAs singly resonant OPO threshold was also very low and its total (signal plus idler) slope efficiency reached 54%. An interesting property of OPGaAs is that due to its high cubic symmetry it can be also pumped with two orthogonal polarizations [55]: This was confirmed by converting the output polarization of a first stage PPLN OPO into circular or pseudo-depolarized, observing that in both cases the threshold of the OPGaAs OPO stage remained low and almost unchanged.

Summarizing, tandem OPOs have produced slightly inferior energies and powers in comparison with 2-μm laser pumped OPOs but at present both concepts are quite comparable in their overall potential with the limits in both cases set by optical damage.

DFG with nanosecond pulses is less demanding than OPO and it is easier to avoid optical damage because there is no resonated wave. Also wavelengths well into the absorption band have been generated as an extension of the long wavelength limit which is difficult for OPOs because of the decreasing parametric gain. Although some of the first DFG experiments on the nanosecond scale employed combinations of a ruby or Nd:YAG with a dye laser, two dye lasers, or dual-wavelength Nd:YAG or CO_2 lasers, using Ag_3AsS_3, AGS, GaSe and CGA as NLCs, it was immediately clear that mixing the output of an OPO has the advantages of simultaneous availability of synchronized in time signal and idler and convenient tuning capability. Thus, in the 1970-ies, nanosecond OPOs based on Ag_3AsS_3 or $LiNbO_3$ were used for DFG in Ag_3AsS_3, AGSe, CdSe, and GaSe. More recently, DFG was demonstrated with combinations of $KNbO_3$ OPO (in AGSe), KTP (type-II interaction in KTP provides narrower linewidths for the mixing) OPO (in AGSe, ZGP, CdSe), and PPLN OPO (in AGS, AGSe, ZGP, GaSe). Normally the long wavelength limits reach 12 μm (AGS and ZGP) and 18 μm (AGSe). Single-frequency operation with <0.1 cm^{-1} linewidth is possible [56] but at low output energies (<100 μJ at 6 μm). Typically the linewidths vary from 1 to 20 cm^{-1} [57]. Spectral narrowing of the OPO output, in relation to the spectral acceptance of the DFG stage, was shown to increase the DFG efficiency [57]: Thus, using AGSe in the DFG stage, the energy at 7.5 μm increased from 380 to 630 μJ and the quantum efficiency reached 16% when the $LNbO_3$ OPO operating at 30 Hz was injection seeded. Energies of the same order were achieved with AGSe also for spectral linewidths <0.1 cm^{-1} at 6 μm, however, this system, operating at 10 Hz, was more complex, involving also a dye laser and intermediate OPA stage before the DFG [58]. The highest DFG energies were obtained with a set-up employing PPLN based OPO and OPA pumped by the same Nd:YAG laser in the one (pump) arm and a dye-laser pumped by the second harmonic of another Nd:YAG laser, followed by DFG with the fundamental in the second (signal) arm [59]: With two walk-off compensated ZGP crystals in the final DFG stage, 2 mJ at 10 Hz were obtained at 5.1 μm with a linewidth of 1.6 cm^{-1} and the tunability extended from 4.6 to 11.2 μm. Even higher energies were obtained with ZGP used as an OPA [60]: In this system, starting from a 500 mJ Nd:YAG laser operating at 10 Hz, the pump arm at 2.08 μm comprised KTP based OPO and OPA and the signal arm – a $KTiOAsO_3$ OPO tunable between 2.8 and 3.7 μm. The ZGP OPA, pumped with 75 mJ and seeded with 0.3 mJ at the signal wave, generated idler between 4.7 and 8 μm with a maximum energy of 8 mJ at 8 μm and total energy (signal plus idler in the 3–5 μm range) of 33 mJ.

The long wavelength limit of DFG was extended by applying CdSe and GaSe for mixing Nd:YAG laser radiation with the idler output of an OPO at 10 Hz: Wavelengths as long as 38.4 μm (<10 THz) were reached with phase-matched DFG in GaSe [61]. Other SSL sources used for nanosecond DFG include combinations of Nd:YAG or alexandrite laser with LiF color center lasers (in AGS and GaSe) [62], Nd:YAG and Ti:sapphire lasers as well as dual-wavelength Ti:sapphire lasers (in AGS and $AgIn_xGa_{1-x}S_2$ which can be used with NCPM) [63].

3.3. Down-conversion of ultrashort pulses

OPGs, OPAs and SPOPOs based on non-oxide NLCs are difficult to realize in the picosecond regime and even more difficult with femtosecond pulses. The major restriction comes not only from the TPA. Powerful femtosecond laser sources operate near 800 nm (Ti:sapphire) and powerful picosecond laser sources – near 1 μm (Nd lasers). More recently powerful femtosecond sources emerge also near 1 μm (Yb lasers). Other ultrashort pulse lasers exist, e.g. Cr^{4+}:forsterite or Cr^{4+}:YAG near 1.25 μm and 1.5 μm, respectively, Cr^{2+} lasers above 2 μm or Er^{3+}-lasers near 3 μm, but with few exceptions the output powers are low and in most cases these are mode-locked lasers without amplifiers. For pumping near 1 μm or down to 800 nm, even being below $E_g/2$, the pump wavelength will not be far enough from the bandgap of the NLC and consequently strong dispersion (GVM) will lead to temporal walk-off of the interacting pulses and low parametric gain. Obviously, only thin NLCs can be used with ultrashort pulse lasers and since the gain will not be sufficient, this is mostly DFG. As an alternative, cascaded schemes could be applied to transform the pump wavelength to spectral ranges of lower dispersion. When the crystal length is matched to the pulse durations, parametric amplification may be accompanied by pulse compression (as with nanosecond pulses) due to the temporal gain narrowing effect, i.e. the output pulses can be shorter.

The first picosecond OPGs based on non-oxide NLCs, developed in the 1980-ies, were pumped by low repetition rate ~20 ps Nd:YAG amplifiers and utilized two type-I (oo-e) Ag_3AsS_3 or AGS crystals, reaching idler wavelengths of 10 μm in the latter case,

at pulse duration of 8 ps [64]. Already in those early experiments the difficulties in controlling the spectral linewidth across the tuning range with such traveling-wave type parametric devices became evident. The next picosecond OPGs that emerged were based on ZGP due to the Er^{3+}:YAG (2.94 μm) or Er^{3+}:YSGG (2.79 μm) pump sources available. These single pass single crystal OPGs were then optimized and with ~100 ps pump pulses following at 1–2 Hz, yielded tunability up to 10 μm with ZGP and 18 μm with GaSe [65]. Not far from degeneracy, the 42-mm long type-II ZGP crystal provided output energies of the order of 100 μJ at quantum efficiency of 17.6%. Further development included double-pass through the same crystal to decrease the output beam divergence and comparison of type-I and type-II ZGP and GaSe crystals [66]. Type-II interaction was characterized by much narrower and almost constant spectral linewidths across the tuning range, down to ~10 cm^{-1}, which is still roughly 50 times above the Fourier limit. With a 40-mm long ZGP crystal, the OPG threshold was ~100 MW/cm^2. The idler tunability was extended with GaSe reaching 19 μm and also an OPG with a 50-mm long type-II CdSe (idler up to 13 μm) was demonstrated. With uncoated crystals the quantum efficiency of the double-pass setup was typically 5–10% and CdSe was superior in the 8–12 μm range.

Er-lasers exhibit relatively long pulse durations because they are only actively mode locked. To obtain shorter pulse durations one obviously has to rely on cascaded schemes, first transforming the wavelength, e.g. of Ti:sapphire amplifiers operating in the 800-nm spectral range. The only demonstration of such a femtosecond OPG operating at 1 kHz was with a 2 mm ZGP type-I crystal in a single pass arrangement [67], Fig. 11a. At 2.07 μm the pump pulse (idler from a BBO based OPG) was 140 fs long and the OPG threshold in ZGP was 25 GW/cm^2. At pump intensity of 60 GW/cm^2, the ZGP OPG produced a total (signal plus idler) output of 215 nJ from an incident pump energy of 16 μJ. The recorded spectra are shown in Fig. 11b. Assuming the same time-bandwidth product for the idler as for the pump (0.5), from the spectral width one can calculate an idler pulse duration of 200 fs near 6.2 μm.

Another cascaded scheme employed a picosecond Ti:sapphire regenerative amplifier operating at 10 Hz and a $LiNbO_3$ seeded OPA as a first stage [68]. The idler pulse of this OPA, tunable near 3.15 μm with duration of 2.7 ps, was used to pump a 10-mm type-II ZGP in double-pass arrangement. The threshold for detection of the parametric fluorescence was less than 100 MW/cm^2. Extraction of 4 μJ (signal plus idler) was measured for an incident pump energy of ~50 μJ. Tunability between 5 and 11 μm (at the 10% energy level) was achieved. The spectral linewidth was <50 cm^{-1} and the generated mid-IR pulses were almost transform limited. Their pulse durations were estimated from cross-correlation measurements with a small fraction of the 795 nm radiation from the Ti:sapphire amplifier, Fig. 12 shows the result

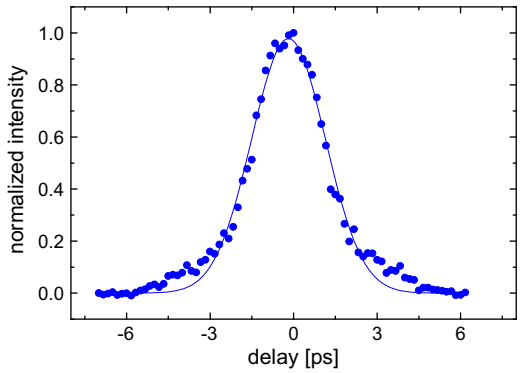

Fig. 12. Cross-correlation trace of the idler from the ZGP OPG at 7.6 μm obtained by SFG with 795 nm pulses.

for the idler at 7.6 μm obtained with pumping at 3.34 μm. From deconvolution of such traces, pulse durations of the order of 1 ps for the whole tuning range (signal and idler) were deduced.

OPG was demonstrated also with the high gain material CGA but it required yet longer pump wavelengths. A Free-Electron-Laser at ~5 μm operating in the burst mode (~100 micropulses of ~600 fs pulse duration separated by 40 ns in a ~4 μs long macropulse) was employed as a pump [69]. With a 7-mm long type-I CGA, the threshold was about 3 GW/cm^2. Tuning between 7 and 18 μm was achieved with typical internal quantum efficiency of 3%.

Seeded OPAs are less demanding than OPGs since they operate far more safely below the damage threshold and seeding enables better control of the spatial and spectral properties. Especially in picosecond systems, seeding helps to avoid excessive spectral broadening while in the femtosecond regime the spectral properties are normally determined by the parametric gain bandwidth but seeding helps to reduce the threshold. However, in most of the cases seeding is applied at the signal wavelength and due to imperfect and not exactly known overlap with the pump, it is difficult to evaluate accurately the amplification factor. Since this factor is normally not very high and the main interest is in the idler generated, this type of OPAs will be discussed within the DFG part following below.

For down-conversion of low energy ultrafast laser sources operating at high repetition rates, as already mentioned, the concept is SPOPO, normally singly resonant for the signal wave. However, the tight focusing required and the TPA, have not allowed yet a SPOPO based on non-oxide material to be pumped at 800 nm with femtosecond lasers. The shortest wavelength used so far for pumping was 1064 nm, from picosecond Nd:YAG laser systems. Unfortunately, AGS that was used at 1064 nm, although free of TPA, has

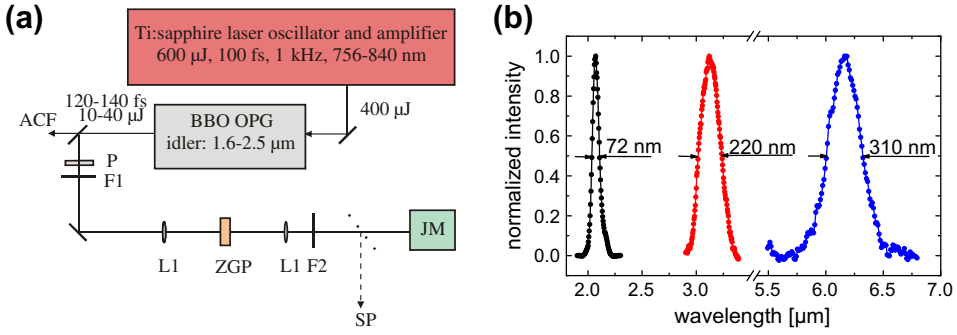

Fig. 11. (a) Experimental setup of the femtosecond ZGP OPG: P, polarizer, F, filters, L, lenses, JM, joule-meter, SP, spectrometer, ACF, autocorrelation function. (b) Spectra of the pump (at 2.07 μm), signal, and idler.

poor thermo-mechanical characteristics. Three concepts to reduce the load to the nonlinear material in terms of average power have been implemented so far: mechanical chopper, Q-switching in addition to mode-locking of the pump laser, and pulsed Nd-YAG oscillator-amplifier system with flashlamp-pumping. In all cases this leads to operation in the burst mode but none of these systems became practical because of cumulative damage problems with AGS. Recently the last approach was implemented with a 9.5-mm CSP crystal in NCPM configuration [70] and no damage was observed. The pump source operated at 25 Hz (macropulses) and 100 MHz (15–20 ps long micropulses), with average power of about 3 W, i.e. 0.12 J per macropulse. The macropulse duration is 2 μs (200 micropulses of 0.6 mJ each). The CSP SPOPO threshold corresponded to an average pump power of 15 mW or a single (micro)pulse energy of 3 μJ.

The incident pump power was limited to slightly above 300 mW because strong pump depletion, reaching typically >40%, was observed starting from about 100 mW of pump power, Fig. 13a. However, no signs of TPA are seen. Fig. 13b shows the input–output characteristics. The maximum idler power of 14 mW corresponds to a single (micro)pulse energy of 2.8 μJ. Only normal incidence was studied in slightly noncollinear geometry and the idler wavelength was ~6.4 μm. The idler pulse had a FWHM of 12.6 ps, from autocorrelation measurements.

In few other cases cw operation based on non-oxide materials has been reported at longer pump wavelengths using tandem SPOPOs. Idler tuning between 4.1 and 7.9 μm with average power reaching 35 mW (~270 pJ at 5.25 μm) at 82 MHz was achieved by pumping a AGSe SPOPO with the signal (at 1.55 μm) from a femtosecond $CsTiOAsO_3$ SPOPO, in turn pumped by a mode-locked Ti:sapphire laser [71]. Idler pulse durations in the 300–640 fs range were estimated. Another SPOPO was based on NCPM in type-II CdSe pumped and tuned by the signal from a PPLN SPOPO at 120 MHz [72]: Starting with a Nd:YLF oscillator, this system generated picosecond idler pulses but the wavelength range was limited to 9.1–9.7 μm and the maximum pulse energy was 90 pJ. Finally, very recently a NCPM ZGP SPOPO was demonstrated [73]: It was based on a similar pump source but using the idler output of the PPLN SPOPO near 2.35 μm to pump a type-II ZGP crystal in a cavity where the idler (5.65 to 5.7 μm) was resonated. Up to 820 mW were extracted from the cavity for a pump power of 3.2 W but unfortunately this was mainly the signal output. Note that such cascaded schemes require cavity length stabilization and synchronization of three short pulse devices, a serious problem which is detrimental for long term stability and potential applications.

DFG of ultrashort pulses is a universal method for down-conversion that can be applied with energetic low repetition rate amplified laser sources and with mode-locked oscillators operating at megahertz repetition rates. At the expense of lower conversion efficiency, the signal wave can be a longer pulse or even cw radiation which relaxes the synchronization requirements. The first experiments with Ag_3AsS_3 and AGS date back to the 1980-ies and involved mixing of energetic picosecond Nd-laser pump radiation with down-shifted signal radiation produced by short-pulse dye lasers or intermediate frequency conversion, and covered the wavelength range up to 10 μm, subsequently extended to 18 μm by using GaSe. In later experiments, typically, with a series of nonlinear convertors and AGS in the final stage, driven by 10 Hz, 1064 nm high energy Nd:YAG lasers, idler energies of the order of 100 μJ were generated with the upper wavelength limit reaching 12.9 μm [74,75]. One approach includes pumping of an intermediate stage by the second (or third) harmonic and using its output as a seed signal for the DFG process, pumped by the fundamental. With Nd:glass systems even sub-picosecond (0.7 ps) pulses were obtained by this method using GaSe, tunable up to 20 μm [76]. Another approach is mixing the signal and idler of a near-IR OPG or OPA: with such a seeded KTP OPA, DFG in GaSe and CdSe covered the 3–24 μm spectral range with very high (>50%) quantum efficiency [77,78]: e.g. starting with 11-ps pulses of 8 mJ energy at 1064 nm and 26 Hz, the output energy varied from 40 μJ at 10 μm to 5 μJ at 20 μm [77]. The system in [78] operated at 1 kHz. A SPOPO was employed in [77,78] to seed the intermediate KTP OPA stage. In [79] the SPOPO output was directly used as a seed signal for DFG in AGS, pumped at much lower (i.e. 50 Hz) repetition rate by amplified pulses from Nd:YLF laser: In this case the DFG stage operated at high gain and could be qualified as seeded OPA, this system provided temporal resolution of ~300 fs from 2.7 to 7 μm. In fact, the macropulse structure can be preserved in the process of down-conversion, and the DFG stage can generate idler pulses with the same time format. This was demonstrated in [80] by mixing the signal and idler from a KTP SPOPO in CdSe: The system operated at 25 Hz for the macropulses and each burst consisted of 100 micropulses with a duration of 8 ps, tuning from 10 to 21 μm was achieved with mid-IR average powers in the milliwatt range. An GaSe OPA was even directly pumped by a long cavity Nd:YVO_4 laser operating at 2 MHz [81]: Half of the energy of the 1 μJ, 4 ps pulses was used for pumping the 10 mm long GaSe crystal and the rest – for creating a seed signal. Parametric gain of 10 was estimated for the OPA(DFG) stage, and with 1% quantum conversion efficiency, the idler was measurable, showing tunability between 5 and 12 μm at ~2 ps pulse duration. Similar approaches for DFG on the picosecond scale, as those explained above for the case of energetic pulses at lower repetition rates, could be applied also with high power ~100 MHz oscillators: The first such DFG demonstrations were based on mixing with synchronously pumped dye lasers but mixing with SPOPO or mixing

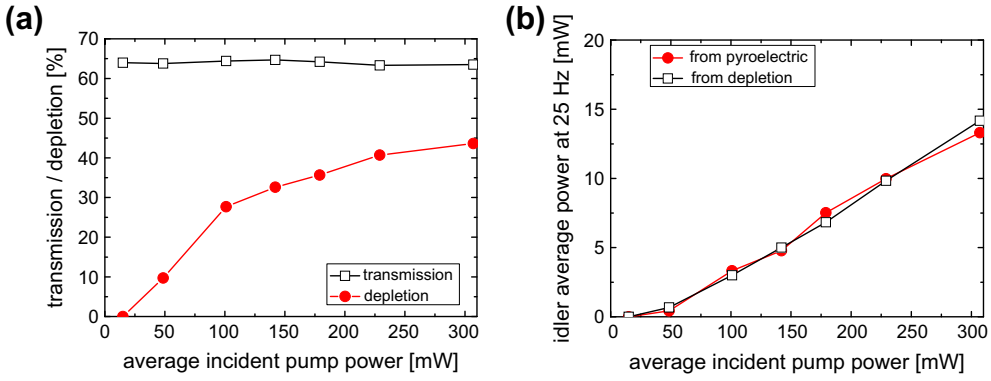

Fig. 13. (a) Pump depletion of the CSP SPOPO and crystal transmission at 1064 nm versus pump power and (b) idler power versus pump power.

of its signal and idler can be used to build an all-solid-state mid-IR system operating at high repetition rates.

DFG at longer input wavelengths, to utilize the high FM of CGA, was demonstrated in [82] using the ZGP based OPG pumped by an Er-laser: Mixing the 90 ps signal and idler pulses from the OPG, the DFG stage produced tunable picosecond pulses between 6.8 and 20.1 μm.

With the advance of Ti:sapphire laser technology in the 1990-ies, both oscillators at ~100 MHz and amplifiers at ~0.01–100 kHz repetition rates, the interest in DFG moved to the femtosecond time domain. High average power Ti:sapphire lasers mode-locked at ~100 MHz offer few possibilities for DFG. Dual-wavelength operation enabled to cover the wavelength region from 7.5 to 12.5 μm with AGS at pulse durations ranging from 450 to 650 fs and average power of 5 μW at 10 μm [83]. Tuning up to 11.5 μm with average power of 15 μW above 9 μm was obtained by mixing two synchronized Ti:sapphire lasers operating at 100 MHz [84]. Much higher average power (>100 μW up to 5 μm) was obtained by mixing the signal and idler from an intermediate near-IR SPOPO [85], while AGSe and GaSe extended the wavelength limit to 18 μm [86,87]. The average powers in [87] were in excess of 1 mW in the 8 μm range, using either GaSe or AGS.

To generate energetic femtosecond pulses in the mid-IR, Ti:sapphire amplifiers can be used. The first DFG systems based on this technology employed traveling-wave dye lasers to generate a synchronized in time signal wavelength. All-solid-state systems were based on similar approaches as those described for oscillators. Dual-wavelength operation has been demonstrated also for Ti:sapphire amplifiers operating at 10 Hz [88]: However, the tuning achieved was confined to the 10 μm spectral range, with maximum energy of 7.4 μJ, starting with a total energy of ~5 mJ, and the pulse duration was of the order of 500 fs. Extension to 20 μm was reported with GaSe at 500 Hz [89]. DFG could be pumped directly by the Ti:sapphire amplifier output but seeding was required for this (seeded OPA) because OPG threshold could not be reached with materials exhibiting no TPA near 800 nm such as the Li NLCs in Table 2 [90]. White-light continuum was generated for this purpose in a 2-mm thick sapphire plate (Fig. 14a). In fact, comparison of different NLCs showed that not only the FM but also the bandgap and the related TPA and dispersive properties are essential for the conversion efficiency, see Fig. 14b, [17]. Crystals of $AgGaGeS_4$ and $Cd_xHg_{1-x}Ga_2S_4$ were also employed in the same arrangement. The latter one, with its much higher FM, yielded also the highest energy output, 2 μJ at 6.6 μm, and also the shortest pulses, ~215 fs estimated from cross-correlation measurements [91].

The concept of mixing the signal and idler from an intermediate near-IR OPG or OPA (normally based on BBO or LBO crystals) turned out to be much more flexible and compatible with shorter pulse durations. For the first time such an all-solid-state system was realized in [92], with a 1 kHz pump system and AGS used in the DFG stage, see Fig. 15. Continuous tunability from 3.3 to 10 μm was achieved with pulse durations of ~160 fs, starting with sub-100 fs signal and idler pulses from the near-IR OPG. This arrangement was further developed by several groups using more powerful pump sources with shorter pulse durations as well as other NLCs. Maximum energies of 9 μJ near 4 μm and >1 μJ in the entire tuning range up to 12 μm were reported in [93] where HGS was also employed as a NLC, Fig. 16a. With shorter pump pulses, 84 fs idler pulses were obtained near 5 μm (Fig. 16b) at an energy level of 0.5 mJ using the mixed crystal $AgGaGe_5Se_{12}$ in the DFG stage [94].

In all cases the pulse durations were only slightly above the Fourier limit. Almost Fourier limited pulses of 54 fs were obtained in [95] where also the spectral range was extended to 20 μm using GaSe. An order of magnitude higher energies (>15 μJ in the whole tuning range of AGS and GaSe and >100 μJ near 4 μm) could be obtained with more powerful Ti:sapphire amplifiers operating at

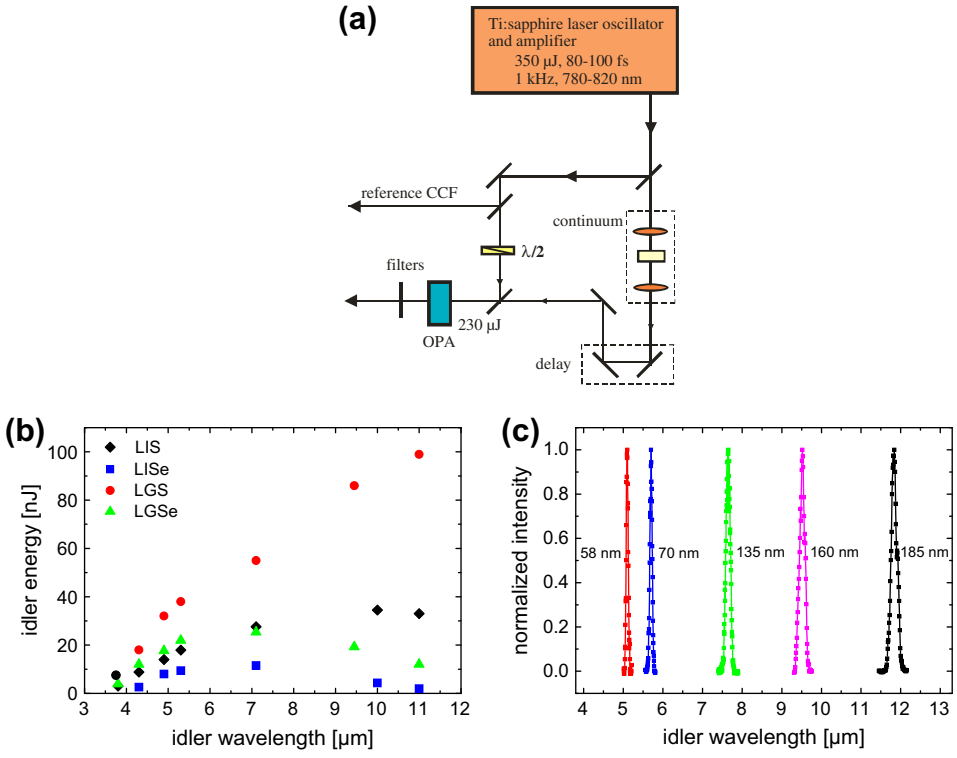

Fig. 14. (a) Experimental setup of the continuum-seeded OPA: λ/2, half-wave plate, CCF, cross-correlation function, (b) idler energies obtained with 3-mm samples of the four Li-NLCs studied, and (c) mid-IR spectra recorded with LIS showing tuning up to 12 μm.

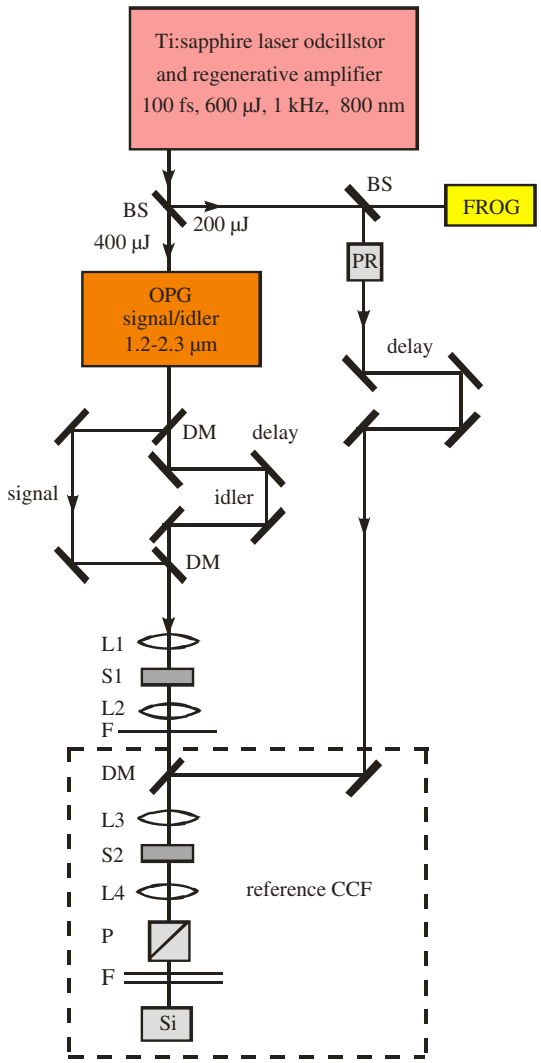

Fig. 15. Experimental setup of DFG from signal and idler of a femtosecond near-IR OPG: DM, dichroic mirrors, PR, polarization rotation, BS, beam splitters, L, lenses, F, filters, S1, DFG crystal, S2, crystal for SFG with a reference beam, P, polarizer, Si, silicon photodiode, CCF, cross-correlation function.

1 kHz, albeit at ~130 fs pulse durations [96]. On the other hand, the same approach is applicable also to Ti:sapphire amplifiers operating up to their 250 kHz limit, although the energy is 40 nJ at maximum when using AGS [97].

It should be emphasized that for sub-100 fs mid-IR pulses, pulse broadening by the group velocity dispersion in optical elements, including the DFG crystal, becomes significant and compensation or pre-compensation of this effect is necessary in order to compress the output pulses and achieve bandwidth-limited pulse durations [95,98]. Such pulse shaping can be performed more comfortably in the near-IR prior to the DFG process and can be used then for programmable generation of amplitude and phase-modulated femtosecond pulses in the mid-IR, interesting for molecular vibrational spectroscopy [99].

The extremely short pulses available from Ti:sapphire lasers enable also DFG of different portions from the same spectrum, possible primarily with oscillators or cavity dumped oscillators because TPA is difficult to avoid with amplified pulses near 800 nm. Thus, 13 fs pulses centered at 780 nm (2 MHz repetition rate) were mixed in GaSe to generate tunable sub-100 fs pulses in the 7–20 μm spectral range just varying the phase-matching angle [100]. Controlled shaping prior to the DFG stage is possible in this arrangement, too [101].

Cr:forsterite systems are analog of Ti:sapphire at longer wavelengths but amplifiers have been demonstrated only scarcely and with the NLCs exhibiting no TPA near 1250 nm it was not possible to realize OPG. For an OPA or DFG, a first stage (seeder) was designed, whose idler seeds (at the signal wavelength) the DFG(OPA) stage pumped at 1250 nm (Fig. 17). Type-I and type-II AGS and HGS crystals were compared, with HGS yielding idler tunability up to 9 μm [102]. The output energies were increased by a factor of 6 (to 4 μJ near 6 μm) by using noncollinear interaction which improves the parametric gain bandwidth and enables the use of longer crystals [103], still at typical pulse durations of 300 fs.

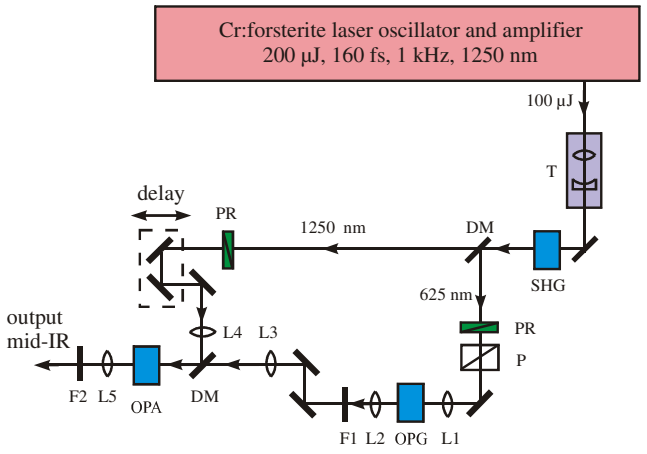

Fig. 17. Experimental setup of mid-IR OPA based on Cr:forsterite pump source: T, telescope, OPG, first stage (seed), OPA, DFG stage, P, blocking polarizer, L, lenses, PR, polarization rotation, F, filters, DM, dichroic mirrors.

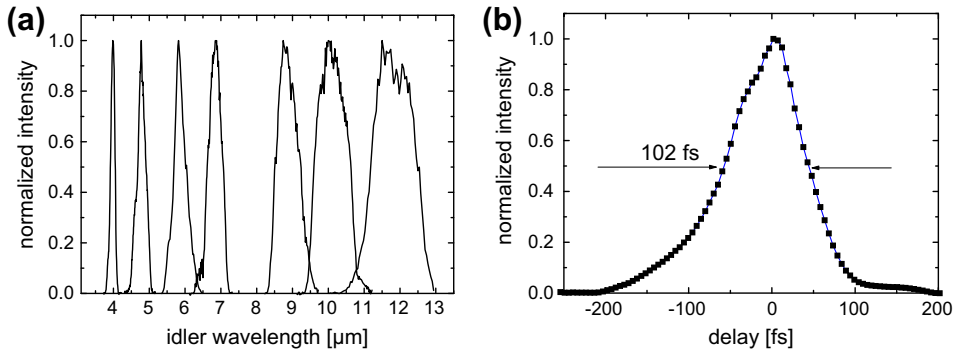

Fig. 16. (a) Idler tuning obtained by DFG with HGS and (b) cross-correlation trace for estimation of the idler pulse duration for DFG performed in $AgGaGe_5Se_{12}$.

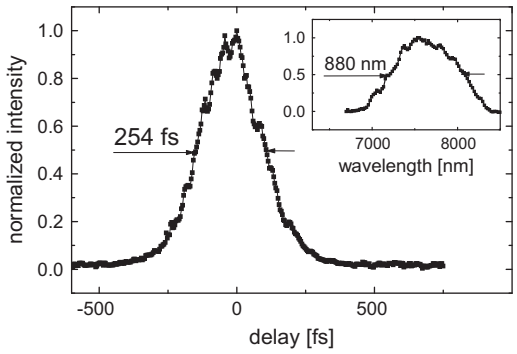

Fig. 18. Cross-correlation trace (SFG with 1250 nm reference pulses) and spectrum (inset) for characterization of the idler pulses at 7.5 μm obtained by DFG with a Cr:forsterite regenerative amplifier operating at 1 kHz.

Shorter pulses (<200 fs), at improved efficiency, could be generated with the mixed $Cd_xHg_{1-x}Ga_2S_4$ crystal which exhibits lower group velocity mismatch due to increased bandgap [104], Fig. 18. LIS was also investigated in a similar experimental setup but did not show essential advantages at a pump wavelength of 1250 nm, presumably because of its low FM.

4. Conclusion

Nonlinear frequency down-conversion is nowadays a powerful method to transform the wavelength of near-IR laser sources to the mid-IR spectral range and generate coherent radiation in all time formats from 3 μm up to 20 μm and above. Non-oxide acentric nonlinear crystals play essential role as a key element in such down-conversion devices, in particular above 5 μm. DFG with non-oxide NLCs seems to lose its importance in the cw regime but is widely used with nanosecond, picosecond, and femtosecond pulses, especially at longer wavelengths where the threshold for OPO, SPOPO, or OPG operation is difficult to achieve because of the decreasing parametric gain. DFG can be quite efficient with ultrashort pulses. Nanosecond OPOs offer great potential for high single pulse energy and high average power in the mid-IR, pumped either by powerful 2-μm lasers or in tandem configurations starting from 1-μm Nd lasers. OPG is difficult to operate in the mid-IR because of the lack of suitable mode-locked and amplified ultrafast laser sources at wavelengths near 2 μm and longer, however, the development of ultrafast Tm^{3+}/Ho^{3+} or Cr^{2+}-based laser systems in the 2–3 μm spectral range could change this situation in the near future. SPOPOs are also plagued by damage and thermal problems related to the nonlinear crystal, and direct pumping near 1 μm is still impossible in the cw regime, but mode-locked oscillators in the 2–3 μm spectral range would make it possible to use nonlinear crystals with higher nonlinearity and better thermomechanical properties, and enable cw operation with a single stage instead of tandem arrangement, as common now in the near-IR.

Yet, in all parametric down-conversion device configurations and operating regimes in the mid-IR, major limitations still exist and important challenges still remain, requiring the continued search for alternative new non-oxide nonlinear materials, laser pump sources and innovative design concepts. Development of new and improvement of existing nonlinear crystals will be instrumental for the future progress. Highly nonlinear new materials such as OPGaAs or CSP could enable novel temporal operation regimes, beyond the "nomenclature" used in the present paper, such as sub-nanosecond OPO, nanosecond OPG, or OPG operating at high (megahertz) repetition rates.

Acknowledgements

The author acknowledges financial support from the European Community's Seventh Framework Programme FP7/2007-2011 under Grant Agreement No. 224042. He acknowledges fruitful collaboration and numerous discussions with P. Schunemann (Nashua, USA), L. Isaenko and A. Yelisseyev (Novosibirsk, Russia), V. Badikov and V. Panyutin (Krasnodar, Russia), J.-J. Zondy (Paris, France), as well as the contribution of former and present PhD students (G. Marchev, V. Tyazhev, F. Rotermund, V. Vedenyapin).

References

[1] P.A. Franken, A.E. Hill, C.W. Peters, G. Weinreich, Phys. Rev. Lett. 7 (1961) 118.
[2] J.A. Giordmaine, R.C. Miller, Phys. Rev. Lett. 14 (1965) 973.
[3] S.B. Mirov, V.V. Fedorov, I.S. Moskalev, D.V. Martyshkin, Laser Photon Rev. 4 (2010) 21.
[4] M. Hagemann, H.-J. Weber, Appl. Phys. A 63 (1996) 67.
[5] A.G. Jackson, M.C. Ohmer, S.R. LeClair, Infrared Phys. Technol. 38 (1997) 233.
[6] D.N. Nikogosyan, Nonlinear Optical Crystals: A Complete Survey, Springer, 2005.
[7] V.G. Dmitriev, G.G. Gurzadyan, D.N. Nikogosyan, Handbook of Nonlinear Optical Crystals, Third Revised ed., Springer, 1999.
[8] W. Jantz, P. Koidl, W. Wettling, Appl. Phys. A 30 (1983) 109.
[9] D. Haertle, M. Jazbinsek, G. Montemezzani, P. Günter, Opt. Express 13 (2005) 3765.
[10] V. Petrov, V.L. Panyutin, A. Tyazhev, G. Marchev, A.I. Zagumennyi, F. Rotermund, F. Noack, Laser Phys. 21 (2011) 774.
[11] V. Petrov, V. Badikov, V. Panyutin, Quaternary nonlinear optical crystals for the mid-infrared spectral range from 5 to 12 micron, in: M. Ebrahim-Zadeh, I. Sorokina (Ed.), Mid-Infrared Coherent Sources and Applications, NATO Science for Peace and Security Series – B: Physics and Biophysics, Springer, 2008, pp. 105–147.
[12] V. Badikov, K. Mitin, F. Noack, V. Panyutin, V. Petrov, A. Seryogin, G. Shevyrdyaeva, Opt. Mater. 31 (2009) 590.
[13] V. Petrov, F. Noack, I. Tunchev, P. Schunemann, K. Zawilski, Proc. SPIE 7197 (2009) 71970M.
[14] J.-J. Zondy, V. Petrov, A. Yelisseyev, L. Isaenko, S. Lobanov, Orthorhombic crystals of lithium thioindate and selenoindate for nonlinear optics in the mid-IR, in: M. Ebrahim-Zadeh, I. Sorokina (Ed.), Mid-Infrared Coherent Sources and Applications, NATO Science for Peace and Security Series – B: Physics and Biophysics, Springer, 2008, pp. 67–104.
[15] S. Fossier, S. Salaün, J. Mangin, O. Bidault, I. Thenot, J.-J. Zondy, W. Chen, F. Rotermund, V. Petrov, P. Petrov, J. Henningsen, A. Yelisseyev, L. Isaenko, S. Lobanov, O. Balachninaite, G. Slekys, V. Sirutkaitis, J. Opt. Soc. Am. B 21 (2004) 1981.
[16] V. Petrov, J.-J. Zondy, O. Bidault, L. Isaenko, V. Vedenyapin, A. Yelisseyev, W. Chen, A. Tyazhev, S. Lobanov, G. Marchev, D. Kolker, J. Opt. Soc. Am. B 27 (2010) 1902.
[17] V. Petrov, A. Yelisseyev, L. Isaenko, S. Lobanov, A. Titov, J.-J. Zondy, Appl. Phys. B 78 (2004) 543.
[18] L. Isaenko, P. Krinitsin, V. Vedenyapin, A. Yelisseyev, A. Merkulov, J.-J. Zondy, V. Petrov, Cryst. Growth Des. 5 (2005) 1325.
[19] V. Badikov, D. Badikov, G. Shevyrdyaeva, A. Tyazhev, G. Marchev, V. Panyutin, V. Petrov, A. Kwasniewski, Phys. Status Solidi (RRL) 5 (2011) 31.
[20] P.S. Kuo, M.M. Fejer, in: M. Ebrahim-Zadeh, I. Sorokina, Mid-Infrared Coherent Sources and Applications, NATO Science for Peace and Security Series – B: Physics and Biophysics, Springer, 2008, pp. 149–168.
[21] A. Douillet, J.-J. Zondy, Opt. Lett. 23 (1998) 1259.
[22] V. Petrov, C. Rempel, K.-P. Stolberg, W. Schade, Appl. Opt. 37 (1998) 4925.
[23] W. Chen, G. Mouret, D. Boucher, Appl. Phys. B 67 (1998) 375.
[24] U. Simon, F.K. Tittel, L. Goldberg, Opt. Lett. 18 (1993) 1931.
[25] E.J. Canto-Said, M.P. McCann, P.G. Wigley, G.J. Dixon, Opt. Lett. 20 (1995) 1268.
[26] S. Vasilyev, S. Schiller, A. Nevsky, A. Grisard, D. Faye, E. Lallier, Z. Zhang, A.J. Boyland, J.K. Sahu, M. Ibsen, W.A. Clarkson, Opt. Lett. 33 (2008) 1413.
[27] E.O. Amman, J.M. Yarborough, Appl. Phys. Lett. 17 (1970) 233.
[28] V.V. Badikov, A.K. Don, K.V. Mitin, A.M. Seregin, V.V. Sinaiskii, N.I. Shchebetova, T.A. Shchetinkina, Quantum Electron. 37 (2007) 363.
[29] K.L. Vodopyanov, J.P. Maffetone, I. Zwieback, W. Rudermann, Appl. Phys. Lett. 75 (1999) 1204.
[30] V.V. Badikov, A.K. Don, K.V. Mitin, A.M. Seryogin, V.V. Sinaiskiy, N.I. Schebetova, Quantum Electron. 35 (2005) 853.
[31] V. Petrov, P.G. Schunemann, K.T. Zawilski, T.M. Pollak, Opt. Lett. 34 (2009) 2399.
[32] V. Petrov, G. Marchev, P.G. Schunemann, A. Tyazhev, K.T. Zawilski, T.M. Pollak, Opt. Lett. 35 (2010) 1230.
[33] H.R. Lee, J. Yu, N.P. Barnes, Y. Bai, ASSP 2004, Technical Digest, paper TuC3.
[34] M. Schellhorn, M. Eichhorn, C. Kieleck, A. Hirth, C. R. Phys. 8 (2007) 1151.
[35] G. Li, B.-Q. Yao, X.-M. Duan, G.-L. Zhu, Y.-Z. Wang, Y.-L. Ju, Chin. Phys. Lett. 27 (2010) 014207.
[36] P.G. Schunemann, Proc. SPIE 6455 (2007) 64550R.

[37] E. Lippert, G. Rustad, G. Arisholm, K. Stenersen, Opt. Express 16 (2008) 13878.
[38] A. Dergachev, D. Armstrong, A. Smith, T. Drake, M. Dubois, Proc. SPIE 6875 (2008) 687507.
[39] L.A. Pomeranz, P.A. Ketteridge, P.A. Budni, K.M. Ezzo, D.M. Rines, E.P. Chicklis, ASSP 2003, OSA TOPS, vol. 83, pp. 142–156.
[40] D. Creeden, P.A. Ketteridge, P.A. Budni, S.D. Setzler, Y.E. Young, J.C. McCarthy, K. Zawilski, P.G. Schunemann, T.M. Pollak, E.P. Chicklis, M. Jiang, Opt. Lett. 33 (2008) 315.
[41] C. Kieleck, M. Eichhorn, A. Hirth, D. Faye, E. Lallier, Opt. Lett. 34 (2009) 262.
[42] A.A. Davydov, L.A. Kulevskii, A.M. Prokhorov, A.D. Savel'ev, V.V. Smirnov, A.V. Shirkov, Opt. Commun. 9 (1973) 234.
[43] R.G. Wenzel, G.P. Arnold, Appl. Opt. 15 (1976) 1322.
[44] T.H. Allik, S. Chandra, D.M. Rines, P.G. Schunemann, J. Andrew Hutchinson, R. Utano, Opt. Lett. 22 (1997) 597.
[45] K.L. Vodopyanov, F. Ganikhanov, J.P. Maffetone, I. Zwieback, W. Ruderman, Opt. Lett. 25 (2000) 841.
[46] W.S. Pelouch, G.J. Wagner, T.J. Carrig, W.J. Scharpf, ASSL 2001, OSA TOPS, vol. 50, pp. 670–674.
[47] S. Chandra, T.H. Allik, R. Utano, J. Andrew Hutchinson, Appl. Phys. Lett. 71 (1997) 584.
[48] E. Cheung, S. Palese, H. Injeyan, C. Hoefer, J. Ho, R. Hilyard, H. Komine, J. Berg, W. Bosenberg, ASSL 1999, OSA TOPS, vol. 26, pp. 514–517.
[49] P.B. Phua, B.S. Tan, R.F. Wu, K.S. Lai, L. Chia, E. Lau, Opt. Lett. 31 (2006) 489.
[50] M. Henriksson, L. Sjöqvist, G. Strömqvist, V. Pasiskevicius, F. Laurell, Proc. SPIE 7115 (2008) 71150O.
[51] D.G. Lancaster, Opt. Commun. 282 (2009) 272.
[52] K.L. Vodopyanov, P.G. Schunemann, Opt. Lett. 28 (2003) 441.
[53] P.B. Phua, K.S. Lai, R.F. Wu, T.C. Chang, Opt. Lett. 23 (1998) 1262.
[54] K.L. Vodopyanov, O. Levi, P.S. Kuo, T.J. Pinguet, J.S. Harris, M.M. Fejer, B. Gerard, L. Becouarn, E. Lallier, Opt. Lett. 29 (2004) 1912.
[55] P.S. Kuo, K.L. Vodopyanov, M.M. Fejer, X. Yu, J.S. Harris, D.F. Bliss, D. Weyburne, Opt. Lett. 32 (2007) 2735.
[56] W.R. Bosenberg, D.R. Guyer, J. Opt. Soc. Am. B 10 (1993) 1716.
[57] S. Haidar, H. Ito, Opt. Commun. 171 (1999) 171.
[58] M. Gerhards, Opt. Commun. 241 (2004) 493.
[59] J. Saikawa, M. Miyazaki, M. Fujii, H. Ishizuki, T. Taira, Opt. Lett. 33 (2008) 1699.
[60] M.W. Haakestad, G. Arisholm, E. Lippert, S. Nicolas, G. Rustad, K. Stenersen, Opt. Exp. 16 (2008) 14263.
[61] W. Shi, Y.J. Ding, Appl. Phys. Lett. 84 (2004) 1635.
[62] A.O. Okorogu, S.B. Mirov, W. Lee, D.I. Crouthamel, N. Jenkins, A.Yu. Dergachev, K.L. Vodopyanov, V.V. Badikov, Opt. Commun. 155 (1998) 307.
[63] S. Banerjee, K. Miyata, K. Kato, N. Saito, S. Wada, Appl. Phys. B 87 (2007) 101.
[64] T. Elsaesser, A. Seilmeier, W. Kaiser, Appl. Phys. Lett. 44 (1984) 383.
[65] K.L. Vodopyanov, J. Opt. Soc. Am. B 10 (1993) 1723.
[66] K.L. Vodopyanov, J. Opt. Soc. Am. B 16 (1999) 1579.
[67] V. Petrov, F. Rotermund, F. Noack, P. Schunemann, Opt. Lett. 24 (1999) 414.
[68] V. Petrov, Y. Tanaka, T. Suzuki, IEEE J. Quantum Electron. 33 (1997) 1749.
[69] K.L. Vodopyanov, G.M.H. Knippels, A.F.G. Van der Meer, J.P. Maffetone, I. Zwieback, Opt. Commun. 202 (2002) 205.
[70] A. Peremans, D. Lis, F. Cecchet, P.G. Schunemann, K.T. Zawilski, V. Petrov, Opt. Lett. 34 (2009) 3053.
[71] S. Marzenell, R. Beigang, R. Wallenstein, Appl. Phys. B 69 (1999) 423.
[72] M.A. Watson, M.V. O'Connor, D.P. Shepherd, D.C. Hanna, Opt. Lett. 28 (2003) 1957.
[73] J.-P. Dherbecourt, A. Godard, M. Raybaut, J.-M. Melkonian, M. Lefebvre, Opt. Lett. 35 (2010) 2197.
[74] H.J. Bakker, J.T.M. Kennis, H.J. Kop, A. Lagendijk, Opt. Commun. 86 (1991) 58.
[75] H.-J. Krause, W. Daum, Appl. Phys. B 56 (1993) 8.
[76] I.M. Bayanov, R. Danielius, P. Heinz, A. Seilmeier, Opt. Commun. 113 (1994) 99.
[77] A. Dhirani, P. Guyot-Sionnest, Opt. Lett. 20 (1995) 104.
[78] K. Finsterbusch, A. Bayer, H. Zacharias, Appl. Phys. B 79 (2004) 457.
[79] R. Laenen, K. Simeonidis, C. Rauscher, IEEE J. Sel. Top. Quantum Electron. 2 (1996) 487.
[80] A.A. Mani, Z.D. Schultz, A.A. Gewirth, J.O. White, Y. Caudano, C. Humbert, L. Dreesen, P.A. Thiry, A. Peremans, Opt. Lett. 29 (2004) 274.
[81] G.I. Petrov, K.L. Vodopyanov, V.V. Yakovlev, Opt. Lett. 32 (2007) 515.
[82] K.L. Vodopyanov, P.G. Schunemann, Opt. Lett. 23 (1998) 1096.
[83] M.R.X. de Barros, R.S. Miranda, T.M. Jedju, P.C. Becker, Opt. Lett. 20 (1995) 480.
[84] S.M. Foreman, D.J. Jones, J. Ye, Opt. Lett. 28 (2003) 370.
[85] J.D. Kafka, M.L. Watts, J.W. Pieterse, R.L. Herbst, Appl. Phys. B 60 (1995) 449.
[86] J.N. Fraser, D. Wang, A. Hache, G.R. Allan, H.M. van Driel, Appl. Opt. 36 (1997) 5044.
[87] S. Ehret, H. Schneider, Appl. Phys. B 66 (1998) 27.
[88] J.F. Xia, J. Song, D. Strickland, Opt. Commun. 206 (2002) 149.
[89] J.M. Fraser, I.W. Cheung, F. Legare, D.M. Villeneuve, J.P. Likforman, M. Joffre, P.B. Corkum, Appl. Phys. B 74(Suppl.) (2002) S153.
[90] F. Rotermund, V. Petrov, F. Noack, L. Isaenko, A. Yelisseyev, S. Lobanov, Appl. Phys. Lett. 78 (2001) 2623.
[91] V. Petrov, V. Badikov, V. Panyutin, G. Shevyrdyaeva, S. Sheina, F. Rotermund, Opt. Commun. 235 (2004) 219.
[92] F. Seifert, V. Petrov, M. Woerner, Opt. Lett. 19 (1994) 2009.
[93] F. Rotermund, V. Petrov, F. Noack, Opt. Commun. 185 (2000) 177.
[94] V. Petrov, F. Noack, V. Badikov, G. Shevyrdyaeva, V. Panyutin, V. Chizhikov, Appl. Opt. 43 (2004) 4590.
[95] R.A. Kaindl, M. Wurm, K. Reimann, P. Hamm, A.M. Weiner, M. Woerner, J. Opt. Soc. Am. B 17 (2000) 2086.
[96] A.B. Sugiharto, C.M. Johnson, H.B. De Aguiar, L. Alloatti, S. Roke, Appl. Phys. B 91 (2008) 315.
[97] M.K. Reed, M.K. Steiner-Shepard, IEEE J. Quantum Electron. 32 (1996) 1273.
[98] N. Demirdöven, M. Khalil, O. Golonzka, A. Tokmakoff, Opt. Lett. 27 (2002) 433.
[99] T. Witte, K.L. Kompa, M. Motzkus, Appl. Phys. B 76 (2003) 467.
[100] R.A. Kaindl, F. Eickemeyer, M. Woerner, T. Elsaesser, Appl. Phys. Lett. 75 (1999) 1060.
[101] F. Eickemeyer, R.A. Kaidl, M. Woerner, T. Elsaesser, A.M. Weiner, Opt. Lett. 25 (2000) 1472.
[102] F. Rotermund, V. Petrov, Opt. Lett. 25 (2000) 746.
[103] F. Rotermund, V. Petrov, Jpn. J. Appl. Phys. 40 (2001) 3195.
[104] V. Petrov, F. Rotermund, Opt. Lett. 27 (2002) 1705.